This dissertation has been
microfilmed exactly as received

69-12,086

DICKINSON, Jerold Thomas, 1941-

A STUDY OF THE HYPERFINE STRUCTURE OF THALLIUM MONOBROMIDE BY THE METHOD OF MOLECULAR BEAM ELECTRIC RESONANCE.

The University of Michigan, Ph.D., 1968
Physics, molecular

University Microfilms, Inc., Ann Arbor, Michigan

A STUDY OF THE HYPERFINE STRUCTURE OF THALLIUM MONOBROMIDE BY THE METHOD OF MOLECULAR BEAM ELECTRIC RESONANCE

by

Jerold Thomas Dickinson

A dissertation submitted in partial fulfillment
of the requirements for the degree of
Doctor of Philosophy in
The University of Michigan
1968

Doctoral Committee:

Associate Professor Jens C. Zorn, Chairman
Professor Peter A. Franken
Assistant Professor Robert Kuczkowski
Professor T. Michael Sanders, Jr.
Assistant Professor William L. Williams

A B S T R A C T

A STUDY OF THE HYPERFINE STRUCTURE OF THALLIUM MONOBROMIDE BY THE MOLECULAR BEAM ELECTRIC RESONANCE METHOD

by

Jerold Thomas Dickinson

Chairman: Jens Zorn

The hyperfine structure of the J = 2 and J = 3 rotational states of TlBr has been measured with a molecular beam electric resonance spectrometer. Hyperfine transition frequencies were measured under conditions of very weak electric and magnetic fields, with a line-width of 500 Hz. The hyperfine interaction constants have been determined for $^{205}Tl^{79}Br$, $^{203}Tl^{79}Br$, $^{205}Tl^{81}Br$, and $^{203}Tl^{81}Br$ in the first five vibrational states for J = 2. Similarly, the interaction constants for J = 3, v = 0 in $Tl^{79}Br$ and $Tl^{81}Br$ have been determined, where the spectra of the two thallium isotopes were not resolved.

All of the spectra measured were well described by a hyperfine Hamiltonian containing the bromine quadrupole interaction, the spin-rotation interactions of both the thallium and the bromine nucleus, and the spin-spin interaction between the nuclei (both the tensor and scalar parts).

The bromine octupole interaction was shown to be too small to make a noticeable contribution to the hyperfine energy.

Certain molecular properties were determined from the measured interaction constants (e.g., the ionic character of the molecule) and compared with values for these properties obtained for the other thallium-halides. Also, a test for the existence of false nuclear quadrupole effects was carried out, with no substantial evidence found for such effects.

Changes in the interaction constants with isotopic species and vibrational state were examined and shown to compare favorably with expected changes.

This thesis also contains a discussion of the interaction Hamiltonian for a diatomic molecule such as TlBr, a description of the MBER spectrometer used in this experiment, and a consideration of the focusing properties of TlBr in a 4-pole electric field.

ACKNOWLEDGMENTS

It is a pleasure to acknowledge my sincere appreciation to Professor Jens Zorn for his continued guidance and encouragement in this work, and to my colleague, David Stephenson, for sharing with me the joy of weaning signals out of a somewhat perverse spectrometer.

I would also like to thank:

Fritzi Stephenson, for her assistance as computer programmer,

David Crosby, for his technical help and political discussions,

Bob Hammerle, Ray Van Ausdal, Jim Purdy, and Tom Gamble, for their assistance in taking data,

and Loraine Reish, for her assistance in the preparation of this manuscript.

The support of this research by the U.S. Atomic Energy Commission is also gratefully acknowledged.

Finally, I wish to thank my wife, Rootbeer, even though...

TABLE OF CONTENTS

	Page
ACKNOWLEDGMENTS	ii
LIST OF TABLES	vi
LIST OF FIGURES	vii
Chapter	
I. INTRODUCTION	1
I.A. The Measurement of Hyperfine Structure in Diatomic Molecules	1
I.B. Motivation for the Study of the Thallium-halides	4
I.C. Motivation for the Study of TlBr	5
I.D. Content of Thesis	6
II. THEORY	7
II.A. Vibrational-Rotational Energy of a Diatomic Molecule	7
II.B. The Hyperfine Interactions	9
II.B.1. The Electrostatic Interactions	10
II.B.2. The Magnetic Interactions	16
II.C. Composite Hamiltonian and Matrix Elements	22
II.D. Energy Levels	22
II.E. Observability Criteria	25
II.F. Factors Determining Amplitudes of Observed Transitions	27

Chapter Page

III. APPARATUS 29

III.A. Oven Chamber, Oven Mount, and Oven . . . 29

III.B. Detector 34

III.C. Focusing Fields 36

III.D. Transition Region 39

III.E. Data-taking System 44

III.F. Helmholtz Coils 46

III.G. Operating Conditions 47

IV. RESULTS 49

IV.A. Search Work and Preliminary Measurements. 49

IV.A.1. Low Resolution Search 49

IV.A.2. High Resolution; the Two Thallium Isotopes 50

IV.A.3. J = 1 Spectra 52

IV.B. Determining Line Assignments 53

IV.C. High Resolution Measurements 54

IV.D. Computer Treatment of Data 62

IV.E. Sources and Estimates of Errors 64

IV.F. Calculated Constants 68

V. INTERPRETATION OF RESULTS

V.A. Verification of Hamiltonian 71

V.B. The Quadrupole Interaction 71

V.B.1. The Ionic Character of the Thallium-halides 72

V.B.2. The Dependence of eqQ on v 75

V.B.3. The Dependence of eqQ on J 78

Chapter Page

V.B.4. False Quadrupole Effects 80

V.C. Spin-Rotation Interactions 85

V.C.1. The Magnetic Fields at the Nuclei . . . 85

V.C.2. The Dependence of c_1 and c_2 on Isotope . 88

V.C.3. Vibrational State Dependence of c_1 and c_2 91

V.D. Spin-Spin Interactions 91

V.E. Conclusion 94

Appendix A Rectangular Vacuum Chamber 96

Appendix B Focusing Field Equation 100

Appendix C Effective Aperture of Focusing Field . . . 107

LIST OF REFERENCES 110

LIST OF TABLES

Table		Page
II(1)	Vibration-Rotation Constants for $^{205}Tl^{79}Br$ . .	8
II(2)	Matrix Elements of H_{hfs}	24
III(1)	Operating Conditions	47
IV(1)	TlBr Hyperfine Transition Frequencies: J = 2.	56
IV(2)	TlBr Hyperfine Transition Frequencies: J = 3.	58
IV(3)	J = 2 Hyperfine Interaction Constants for TlBr	69
IV(4)	J = 3, v = 0 Hyperfine Interaction Constants for TlBr	70
V(1)	Ionic Character of Lithium-Halides	73
V(2)	Ionic Character of Thallium-Halides	74
V(3)	Constants Related to Dependence of eqQ on v. .	75
C(1)	Effective Apertures of Focusing Fields and Observed Intensities	108

LIST OF FIGURES

Figure		Page
II(1)	J = 1 Energy Level Diagram for TlBr . . .	23
III(1)	Cutaway Diagram of Apparatus	30
III(2)	Oven Mount and Oven Chamber	32
III(3)	Tube-Oven Installed in Oven Holder, inside Oven Chamber	33
III(4)	4-Pole Focusing Field	37
III(5)	View of C-Field Electrodes with Approximations to the Electric Field Lines Indicated	40
IV(1)	(5/2,2) → (3/2,2) Transition (λ_4) in J = 2, v = 0, TlBr	51
IV(2)	J = 2 Energy Level Diagram for TlBr . . .	60
IV(3)	J = 3 Energy Level Diagram for TlBr . . .	61
IV(4)	Influence of Earth's Magnetic Field on the J = 2, v = 0 (5/2,3) → (1/2,1) Transition (α_2) in $Tl^{79}Br$	65
IV(5)	Effect of Changing V_{dc} and V_{rf} on the J = 2, v = 0 (5/2,3) → (7/2,4) Transition (β_3) in $Tl^{79}Br$	67
V(1)	The Quantity $\Delta = eqQ_{^{203}Tl^{79}Br} - eqQ_{^{205}Tl^{79}Br}$	79
V(2)	Ratios of the Quadrupole Interaction Constants for ^{79}Br in TlBr and the Free Bromine Atom	86

Figure		Page
V(3)	Dependence of c_1 and c_2 on Vibration State for J = 2, $^{205}Tl^{79}Br$	92
A(1)	Rectangular Vacuum Chamber	97
B(1)	Schematic Diagram of Beam Source and 4-Pole Focusing Field	101
B(2)	Graphical Solution to the Trancendental Equation: tan y = L_2/L_1 1/y, for L_2/L_1 in the Neighborhood of 20	105

CHAPTER I

INTRODUCTION

I.A. The Measurement of Hyperfine Structure in Diatomic Molecules

The measurement of the hyperfine interactions in diatomic molecules is of interest because of the information it provides regarding the structure of the molecules. With knowledge of the electric and magnetic moments of the nuclei, hyperfine structure (hfs) measurements allow us to calculate certain properties of the electric and magnetic fields at the nuclear sites. For example, a measurement of the spin-rotation interaction at a particular nucleus allows us to calculate the magnitude of the magnetic field at the nucleus.

The molecular electric and magnetic fields arise from the presence and motion of the charges in the molecule. Hence, in principle, the fields may be calculated if the structure of the molecule is sufficiently understood, i.e., if the wave functions of the molecule are known. In the few light molecules in which these wave functions are known, hfs measurements provide sensitive tests of their accuracy.

To describe the structure of heavier diatomic molecules it is necessary to resort to simplified models. Measurements of hfs often serve either as a test of the model or as a source of information to improve the model. An illustration

of the latter is the use of the quadrupole interaction to probe the character of the chemical bond between the atoms in a diatomic molecule (Townes and Dailey, 1949).

In addition to providing information about the structure of the molecule, precision hfs measurements also provide a means for detecting interactions involving higher order nuclear moments, e.g., the nuclear electric hexadecapole moment or the magnetic octupole moment. Estimates of the magnitudes of these interactions in molecules (Svidzinskii, 1964, p. 131) indicate that they might be barely observable with present day experimental precision.

In diatomic molecules the dominant hyperfine interactions are those involving the electric quadrupole and magnetic dipole moments of the nuclei. The spectrum of transitions between the resulting hyperfine energy levels is simplified if the electronic ground state of the molecule is, to first order, one of zero orbital and zero spin angular momentum. This is the case for the majority of molecules since they have $^1\Sigma$ electronic ground states. For such molecules, the magnetic fields at the site of the nuclei are relatively small (~2 gauss), leading to interaction energies typically from one to 100 kHz. If one or both of the nuclei possess an electric quadrupole moment, their interactions with the gradient of the electric fields within the molecule lead to even larger contributions to the hfs (typically from one to 100 MHz). If only one nucleus has a quadrupole moment and the other nucleus is spin $\frac{1}{2}$ or 0, the spectrum is relatively easy to describe.

One obtains the highest precision measurements of the transition frequencies between hyperfine energy states by means of molecular beam techniques. In observing the transitions while the molecules are in free-flight one avoids any interaction between the molecules, since the density of particles in the beam is very low (typically 10^6 particles/cm^3). In addition, Doppler broadening of the observed resonance is to a great extent eliminated because the beam is so unidirectional.

Molecular Beam Electric Resonance (MBER) is a method for observing hyperfine transitions in polar diatomic molecules. It is a modification of Molecular Beam Magnetic Resonance (MBMR), first introduced by I. I. Rabi (1938). At the suggestion of Rabi, the method of MBER was first applied to the study of the hfs in CsF by H. K. Hughes (1949). Extensive discussions of the methods and applications of MBMR and MBER may be found in Ramsey (1956) and in Kusch and Hughes (1959).

Experimentally, the resonances are generally easier to measure under the conditions of very weak external electric and magnetic fields, as opposed, for example, to measurements in high electric field. However, the interpretation of the very weak field spectrum often requires that one ignore unresolved Stark and Zeeman splittings that result in line broadening and in shifting of the apparent line-center. The errors introduced by these effects can usually be made small relative to the apparatus line-width.

I. B. Motivation for the Study of the Thallium-halides

We chose to study the hfs of the thallium-monohalides with a high resolution MBER spectrometer for a number of reasons. First, thallium has a nuclear spin of $\frac{1}{2}$, hence no quadrupole moment. As a result, the hfs of TlCl, TlBr, and TlI are dominated by the single electric quadrupole interaction of the halogen nucleus, thus simplifying the interpretation of their spectra. TlF has no quadrupole interaction because Tl and F both have spin $\frac{1}{2}$ nuclei.*

Second, it had been demonstrated by Gräff (1958) and by Zeiger and Bolef (1952) that beams of TlF and TlCl could be produced and detected. Slight modifications of their methods proved to be quite adequate for making and detecting beams of all the Tl-halides.

Third, the Tl-halides all have reasonably large permanent electric dipole moments. This allows the use of four-pole electric fields to focus particular hyperfine states of the lower rotational states of these molecules onto the detector.

Fourth, microwave studies have been made on all the Tl-halides by Barrett and Mandel (1958) and by Fitzky (1958). Fitzky's work gives approximately one per cent determinations of the halide quadrupole interaction constants. This allows

---

*The hfs of TlF has been studied in great detail under a variety of external field conditions by Dr. Gernot Gräff and collaborators at the Institute of Physics, University of Bonn. [See Gräff (1958), Drechsler (1961), Boeckh (1964)]

us to predict the hyperfine transition frequencies in TlBr and TlI to within ± 1 MHz.*

TlBr and TlI were of particular interest to us because hyperfine transitions had not yet been observed in these molecules. Also, our study of these molecules would, with the inclusion of Gräff's TlF measurements and our TlCl measurements, provide a complete set of accurate hyperfine interaction constants for the entire family of thallium-halides.

I. C. Motivation for the Study of TlBr

There are additional interesting features of thallium bromide that provide further motivation for its investigation. For example, there are four naturally occurring isotopic species of the molecule: $^{205}Tl^{79}Br$, $^{203}Tl^{79}Br$, $^{205}Tl^{81}Br$, and $^{203}Tl^{81}Br$. The relative abundance of the two Tl isotopes is $^{205}Tl/^{203}Tl = 70/30$, whereas the Br isotopes have a relative abundance of 50/50. The nuclear spins of the Tl isotopes are both $\frac{1}{2}$; both of the Br isotopes have spin 3/2. Hence, a measurement of the transition frequencies for all four species allows a comparison of the various hyperfine interaction constants between molecules having the same number of electrons and same nuclear spins, but slightly different nuclear electric and magnetic moments and nuclear masses. For example, there has been reported a ratio of the quadrupole interaction constants for the two bromine isotopes as measured in LiBr

*In the case of TlCl, two low resolution molecular beam studies (Zeiger, 1952; Carlson, 1952) have already been made with sufficient precision to determine the transition frequencies to ± 5 kHz. [Our studies involved measurements of these frequencies to ± 0.1 kHz. (Hammerle, 1968)]

(Hebert, 1964) which differs significantly from the same ratio as measured in the free bromine atom (Brown, 1966). Bonczyk and Hughes (1967) have suggested that this observed difference might be evidence for nuclear polarization. We will look for the same effect in TlBr.

A final interesting feature of TlBr is that it has a fairly small vibrational constant (ω_e = 475 cm^{-1}), which provides a substantial population in the higher vibrational states at the temperature of our source ($\cong$ 500°C). Consequently, a study can be made of the interaction constants as a function of vibrational state.

I. D. Content of Thesis

This thesis is concerned with our measurements of the hfs in TlBr. A short discussion of the theory of the hfs in diatomic molecules with a single quadrupole interaction is presented in Chapter II. The experimental apparatus used in these investigations is described in Chapter III. Chapter IV is concerned with the results of the measurements and with the calculations of the hyperfine interaction constants. In Chapter V these results are interpreted in terms of semi-quantitative models for the hyperfine interactions.

CHAPTER II

THEORY

II. A. Vibrational-Rotational Energy of a Diatomic Molecule

If we neglect for a moment the hyperfine interactions, a diatomic molecule may be considered as a vibrating rotator, with energy levels given by:

$$E_{v,J} = \omega_e \left(v + \tfrac{1}{2}\right) - \omega_e x_e \left(v + \tfrac{1}{2}\right)^2 + \ldots \qquad \text{II(1).}$$

vibrational energy

$$+ B_v J(J+1) - D J^2(J+1)^2 + \ldots$$

rotational energy

where:

$E_{v,J}$ is the energy of the vth vibrational state and Jth rotational state, J being the rotational angular momentum quantum number.

ω_e is the harmonic oscillator vibrational constant, which dominates the vibrational energy.

$\omega_e x_e$ is the first anharmonic correction constant, and is much smaller than ω_e.

D is the centrifugal distortion correction to the rotational energy and takes into account the effect of the stretching of

the bond between the atoms in reaction to the centrifugal force produced by rotation. It is a very small correction, and for our purposes it can be ignored.

B_v is the rotational constant for the vth vibrational state. It is related to the reduced mass of the molecule, m, the internuclear separation, R, and Planck's constant, h, as follows:

$$B_v = h/8\pi^2 mR^2 \qquad \text{II(2).}$$

[$m = M_1M_2/(M_1 + M_2)$, where M_1 and M_2 are the masses of the two atoms in the molecule.] B_v may also be expressed in a power series in $(v + \frac{1}{2})$:

$$B_v = B_e - \alpha_e(v + \tfrac{1}{2}) + \gamma_e(v + \tfrac{1}{2})^2.$$

The measured values of the vibration-rotation constants for $^{205}Tl^{79}Br$ (Fitzky, 1958) are listed in Table II(1).

Table II(1) Vibration-Rotation Constants for $^{205}Tl^{79}Br$

ω_e	=	475 cm^{-1}
$\omega_e x_e$	=	0.39 cm^{-1}
B_e	=	1293879 (8) kHz
α_e	=	3932 (5) kHz
γ_e	=	4.3 (30) kHz
D	=	0.247 kHz

(Errors are shown in () and are in units of last quoted integer. The values of ω_e, $\omega_e x_e$, and D are calculated from B_e, α_e and γ_e.)

A value of R may be calculated using Equation II(2) and the above value of B_e. The resulting value of R is denoted by R_e. R_e is to be identified as the internuclear separation for which the internuclear potential V(R) has its minimum value. Hence, R_e is called the equilibrium internuclear separation. Because of the molecule's vibrational motion, the internuclear separation varies with time. Consequently, quantities which are functions of R must be averaged over this vibrational motion. Since V(R) deviates from a harmonic oscillator potential, the averages of integral powers of R, $\langle R^n \rangle_v$, are not equal to R_e^n. The corrections to R_e^n necessary to obtain $\langle R^n \rangle_v$ may be written in terms of the constants B_e, α_e, and ω_e (see Ramsey, 1956, p. 231). Eq. II(2) contains implicitly the dependence of $\langle 1/R^2 \rangle_v$ on v.

II.B. The Hyperfine Interactions

Hyperfine interactions are those electromagnetic interactions within the molecule that are dependent on the orientation of the nuclear spins relative to the rotational angular momentum, J, and relative to each other. Such interactions result in splittings of the vibrational-rotational energy levels of the molecule. The hyperfine interactions may be described in terms of the nuclear electric and magnetic moments interacting with the electric and magnetic field

moments of the molecule occurring at each nucleus.

II.B.1. The Electrostatic Interactions

The general electrostatic interaction energy between the charge distribution of one of the nuclei (e.g., nucleus 1) and the charges of the molecule external to the nucleus can be described by a multipole expansion (see Ramsey, 1956, pp. 51-67):

$$W_E = \sum_k F^{(k)} \cdot Q^{(k)} . \qquad \text{II(3).}$$

$F^{(k)}$ represents the multipole moment of order 2^k of the electric field at the center of nucleus 1. $Q^{(k)}$ represents the multipole moment of order 2^k of the charge distribution of nucleus 1. Both quantities are kth-rank irreducible spherical tensors having (2k + 1) components.

The k=0 term represents the monopole interaction, and is simply the product of the total charge of nucleus 1, $Z_1 e$, and the electrostatic potential, evaluated at the center of nucleus 1. The magnitude of the monopole interaction is characterized by the spacing of the molecule's electronic states. In diatomic molecules these are typically one to twenty electron volts. Consequently the energy required to excite the molecule out of the electronic ground state is appreciably larger than the thermal energies available in the molecular source, so that all of the beam is in the electronic ground state. The monopole interaction does not contribute to the hfs of the molecule because it involves no angular

dependence of the nuclear charge distribution relative to the rest of the molecule.

The k=1 term of Eq. II(3) is the electric dipole interaction. If we accept the assumption that nuclear wave functions are invariant under coordinate inversion, then the dipole interaction vanishes. ($Q^{(1)}$ is an operator of odd parity; therefore, $\langle \text{Nuclear}| Q^{(1)} |\text{Nuclear}\rangle = 0$.) Several investigators have carefully looked for the existence of nuclear dipole moments. To date, only upper limits for such moments have been established. For example, the dipole moment of the neutron has been shown to be less than 10^{-22} esu-cm. For our purposes, such results imply that there will be no visible contribution to the hfs of diatomic molecules by nuclear electric dipole interactions. Similar arguments insure that electric moments of higher, odd k, will also vanish.

The Nuclear Quadrupole Interaction

The first nonzero electrostatic interaction is therefore the k=2 term in Eq. II(3), the nuclear electric quadrupole interaction. The cylindrical symmetry of the nuclear charge distribution about the spin axis allows a choice of coordinates that cause several of the components of the nuclear quadrupole moment tensor to vanish. The nonzero components may all be defined in terms of a single quantity, Q, called "the" quadrupole moment of the nucleus. Q is a constant which tells us about the departure of the nuclear charge distribution from spherical symmetry. If the charge distribution is elongated along the spin axis, Q is a positive

number; if the charge distribution bulges in the middle and is flattened at the poles, Q is a negative number. Typical values of Q suggest elongations or bulges of nuclear charge distributions on the order of 5% of the nuclear diameter. The majority of nuclear quadrupole moments are positive, a fact nicely explained by the collective model of the nucleus (Townes, 1958). For the two isotopes of bromine, $_{35}Br^{79}$ and $_{35}Br^{81}$, the values of Q are positive, approximately 0.3 x 10^{-24} cm^2 in magnitude, with about a 20% difference between them.

The nuclear quadrupole interaction is generally the largest of the hyperfine interactions. It serves as a coupling between the two angular momenta $\vec{I}_1$ and $\vec{J}$, where $\vec{I}_1$ is the spin angular momentum of the nucleus containing the quadrupole moment, and J is the rotational angular momentum of the molecule. The resultant angular momentum shall be called $\vec{F}_1$, where $\vec{F}_1 = \vec{I}_1 + \vec{J}$. The number of allowed hyperfine energy levels due to the quadrupole interaction is equal to the number of allowed values of F_1, namely $(2I_1 + 1)$ or $(2J + 1)$, whichever is smaller $[|I_1 + J|, |I_1 + J - 1|, \ldots, |I_1 - J|]$.

The contribution to the hyperfine energies by the quadrupole interaction may be calculated by treating the expression $H_{QUAD} = F^{(2)} \cdot Q^{(2)}$ as an additional term in the molecular Hamiltonian. For our purposes, the zeroth order Hamiltonian may be taken as the vibrational-rotational energy of the molecule, which we shall denote by $H_{VIB-ROT}$. In zero external field an appropriate representation for carrying out the

eigenvalue problem is the coupled representation $|\alpha(I_1 J)\ F_1 M_{F_1}\rangle$, where α represents the remaining quantum numbers of the molecule not related to the quadrupole coupling (e.g., the electronic quantum numbers, and v, the vibrational quantum number).

The Hamiltonian matrix elements may be calculated in this representation, and the eigenvalues found by direct diagonalization. However it is usually easier to treat H_{QUAD} as a perturbation on $H_{VIB-ROT}$ and to find the hyperfine energies by means of degenerate, time-independent perturbation theory. The hyperfine energies may then be written as algebraic expressions of the matrix elements found in the above coupled representation.

The matrix elements of the quadrupole interaction have been derived by Benz, Bauder, and Gunthard (1966). Misprints in their results have been corrected by Miller (1967). Their derivation takes advantage of the form of H_{QUAD} as the contraction of two irreducible spherical tensors, whereby methods of Racah may be applied, along with the Wigner-Eckart Theorem. The results are most compactly written in terms of Wigner 3-j and 6-j symbols as follows:

$$\langle \alpha'(I_1\ J')F_1' | F^{(2)} \cdot Q^{(2)} | \alpha(I_1\ J)F_1 \rangle =$$

$$\frac{eqQ}{4} (-1)^{I_1+J+J'+F_1} \delta_{\alpha'\alpha}\, \delta_{F_1'F_1} \sqrt{(2J'+1)(2J+1)} \begin{Bmatrix} F_1 & J' & I_1 \\ 2 & I_1 & J \end{Bmatrix}$$

$$\times \frac{\begin{pmatrix} J' & 2 & J \\ 0 & 0 & 0 \end{pmatrix}}{\begin{pmatrix} I_1 & 2 & I_1 \\ -I_1 & 0 & I_1 \end{pmatrix}} \qquad \text{II(4).}$$

where e is the electron charge, q is the expectation value

of the component of the electric field gradient which lies along the internuclear axis, evaluated in the molecular frame of reference at the center of nucleus 1:

$$q = \langle \alpha | \frac{\partial E_z}{\partial z} | \alpha \rangle .$$

Q is "the" quadrupole moment of nucleus 1. The quantity eqQ is called the quadrupole interaction constant. Properties of the 3-j and 6-j symbols in Eq. II(4) allow us to say the following about the matrix elements of H_{QUAD}:

The matrix elements are symmetric in J and J′.

Non-zero matrix elements occur only for J > 0,

$$J' = J, \text{ and } J' = J \pm 2.$$

Note also that the quadrupole interaction matrix is diagonal in both F_1 and M_{F_1}.

The energy of the F_1 levels relative to the (v,J) energy levels can then be expressed in terms of these matrix elements by the usual perturbation expansion. Through third order these energies are:

$$E_{J,F_1} = \langle J,F_1 | H_{QUAD} | J,F_1 \rangle \qquad (1) \qquad \text{II(5)}$$

$$+ \sum_{J}{}' \frac{|\langle JF_1 | H_{QUAD} | J'F_1 \rangle|^2}{E_J - E_{J'}} \qquad (2)$$

$$\left. + \sum_{J'J''}{}'' \frac{\langle JF_1 | H_{QUAD} | J'F_1 \rangle \langle J'F_1 | H_{QUAD} | J''F_1 \rangle \langle J''F_1 | H_{QUAD} | JF_1 \rangle}{(E_J - E_{J'})(E_J - E_{J''})} \right\} (3)$$

$$\left. + \sum_{J}{}' \frac{\langle JF_1 | H_{QUAD} | JF_1 \rangle |\langle JF_1 | H_{QUAD} | J'F_1 \rangle|^2}{(E_J - E_{J'})^2} \right\}$$

where E_J is the rotational energy of the molecule when the rotational angular momentum of the molecule is equal to J, and the dashes on the summation signs indicate that J′ and J″ are always unequal to J. The numbers in parentheses on the right indicate the order of the various contributions.

If necessary, higher order perturbation corrections can be made when the precision of the hyperfine structure measurements merit such further corrections. The magnitudes of higher order corrections to the diagonal matrix elements (first term of Eq. II(5)) are typically 10^{-2} x eqQ/B x (the preceding correction). For TlBr, eqQ/B is roughly 1/10, and the diagonal elements are about 20 MHz. Second order corrections are about 20 kHz, third order are about 100 Hz, and fourth order are about one or two Hz. Since the hyperfine structure measurements to be discussed later involve uncertainties of about ± 100 Hz, fourth and higher order corrections to the quadrupole energies may be ignored.

The molecular property, q, is dependent on the location of the electrons and the other nucleus, all considered as point charges. For molecules containing heavy atoms, such as thallium and bromine, the electronic wave functions are not known, so that precise calculations of q are not feasible.

There are a few semi-empirical theories developed by Townes and Dailey (1949), Sternheimer (1950), and de Wijn (1966) which together provide a semi-quantitative description of the quadrupole interaction.

All contributions to q are attributed to the covalent structure of the molecule by Townes and Dailey. Sternheimer

bases his calculations on an anti-shielding effect produced by a polarization of the electrons of atom 1, due to the charges of atom 2. De Wijn adds to these effects a partial quenching of polarizations of the electrons in atom 1. The above theories, taken together, allow q to be approximated as a function of properties of the two ions, such as their polarizabilities, and of molecular properties such as the internuclear separation [see Eq. IV(1)]. More shall be said about this model, as applied to the thallium-halides, in Chapter V, Section A. 1.

II.B.2. The Magnetic Interactions

The interactions between the internal magnetic fields of the molecule and the magnetization of the two nuclei lead to further contributions to the hyperfine structure. As in the case of the electrostatic interactions, the magnetic interactions may be expressed by a multipole expansion,

$$W_M = \sum_k H^{(k)} \cdot G^{(k)} \qquad \text{II(6)}$$

where $H^{(k)}$ represents the kth magnetic moment of the nucleus, and $G^{(k)}$ represents the kth multipole moment of the magnetic field at the nucleus. Because of parity arguments, nuclei may possess magnetic moments of odd order only. The magnetic dipole interactions (k=1) in molecules are typically a few kilohertz in magnitude, whereas magnetic octupole interactions (k=3) are expected to be a factor of 10^{-3} smaller, and therefore only a few Hertz in magnitude.

The magnetic dipole interactions are somewhat easier to

interpret when they are developed on the basis of phenomenological arguments rather than a formal tensor product development. We assume the nuclei to possess magnetic dipole moments aligned with their spin angular momentum, and then investigate the possible sources of magnetic fields at each nucleus to arrive at a description of the interaction energies. With only a slight loss of generality, these interactions may be expressed in terms of the angular momentum operators $\vec{I}_1$, $\vec{I}_2$, and $\vec{J}$, and their matrix elements can be calculated in a straightforward manner.

Spin-Rotation Interactions

If a $^1\Sigma$ diatomic molecule is not rotating, the magnetic field throughout the molecule would be zero because the electrons, the only source of field, are paired in such a way that the individual electronic orbital and spin angular momenta cancel one another. However, in the rotating molecule, the electronic state is slightly perturbed by the rotational motion, which introduces a small but significant admixture of higher electronic states (in particular, the excited π states). These excited states do possess non-zero electronic angular momentum and therefore give rise to a small magnetic field. The motion of the "other" nucleus, which appears to rotate about "the" nucleus, also generates a magnetic field and must be included. The sum of these fields, $\vec{H}_{i\ ROT}$, interacts with the magnetic dipole moment of the nucleus, $\vec{\mu}_i$, where the interaction energy is given by $\vec{\mu}_i \cdot \vec{H}_i$. Considering that $\vec{\mu}_i = g_i \vec{I}_i$, (where g_i is the g-factor of the ith nucleus), plus the fact that $\vec{H}_i$ arises from the

rotation of the molecule, it is clear why the above interaction is called the "spin-rotation" interaction.

The spin rotation interaction for a diatomic molecule may be written as:

$$H_{\text{spin-rotation}} = c_i \vec{I}_1 \cdot \vec{J}, \qquad \text{II(7)}$$

where c_i is the spin-rotation interaction constant for the ith nucleus. Models for the spin-rotation interaction have been given by White (1955) and Schlier (1961). In Section V.C. we consider various aspects of such models as applied to the thallium-halides.

The matrix elements of the two spin-rotation interactions may be found in the coupled representation, again by applying methods of Racah and the Wigner-Eckart Theorem to the case of scalar products or irreducible spherical tensors (Edmonds, 1957). The resulting matrix elements are given in Table II(2) in terms of 3-j and 6-j symbols where convenient.

It should be noted that the matrix elements involving c_1 are diagonal in the $|(I_1\ J)F_1\ M_{F_1}\rangle$ representation. The $c_2 \vec{I}_2 \cdot \vec{J}$ interaction introduces a coupling between $\vec{I}_2$ and $\vec{F}_1$ to produce a new total angular momentum $\vec{F} = \vec{F}_1 + \vec{I}_2$. In the case where $I_2 = 1/2$ the possible values of F for each F_1 are $F_1 \pm 1/2$, so that each F_1 level is split into two

F levels by the $\vec{I}_2 \cdot \vec{J}$ interaction. The c_2 interaction has off-diagonal elements in F_1. They introduce corrections to the various F levels which are on the order of c_2^2/eqQ, and in many instances must be included.

Spin-Spin Interactions

The two magnetic dipole moments of the nuclei in the molecule may also interact with each other. This interaction is called the "spin-spin" interaction. The most obvious contribution to the spin-spin interaction is the direct dipole-dipole interaction, which has the form of the classical interaction energy between two magnetic dipole moments:

$$H_{(\text{dipole-dipole})} = \vec{\mu}_1 \vec{\mu}_2 / R^3 - 3(\vec{\mu}_1 \cdot \vec{R})\,(\vec{\mu}_2 \cdot \vec{R})/R^5 \qquad \text{II(8)}$$

where $\vec{\mu}_1$ and $\vec{\mu}_2$ are the nuclear magnetic moments of the two nuclei, and $\vec{R}$ is the vector pointing from nucleus 1 to nucleus 2, with a magnitude, R, equal to the internuclear separation. For a diatomic molecule this can be written in terms of the angular momenta as follows (Ramsey, 1956, p. 205):

$$H_{(\text{dipole-dipole})} = \frac{\mu_1 \mu_2}{R^3} \frac{2[3(\vec{I}_1 \cdot \vec{J})(\vec{I}_2 \cdot \vec{J}) - (\vec{I}_1 \cdot \vec{I}_2)J(J+1)}{(2J-3)(2J+3)} \qquad \text{II(9)}$$

By writing $H_{(\text{dipole-dipole})}$ in this way we have ignored the off-diagonal elements in J. Since the matrix elements are typically less than 100 kHz, whereas rotational energies are on the order of 10GHz, the corrections to the energy due to these off-diagonal elements would be about 10^{-5} Hz and can therefore be ignored.

An additional contribution to the spin-spin interaction

arises from a coupling of the nuclear spins via the electrons of the molecule. (Ramsey, 1953) describes this interaction as being between each nuclear magnetic moment and the electron spin of its atom together with an exchange coupling of the electron spins of the two atoms. In terms of perturbation theory, the above mechanism is a second order perturbation connecting the ground state to excited triplet states of the molecule, where the various nuclear spin-electron spin couplings are the perturbing interactions. Ramsey has shown (Ramsey, 1953) that the electron-coupled nuclear spin-spin interaction in a diatomic molecule can be written:

$$H_{\left(\substack{\text{spin-spin}\\ \text{electron-coupled}}\right)} = \sum_{ij} I_{1i}\, d_{ij}\, I_{2j} + c_4\, \vec{I}_1 \cdot \vec{I}_2 \qquad \text{II(10)}$$

where the first term is the tensor part of the interaction and the second term is the scalar part. d_{ij} is the ij Cartesian component of a traceless tensor of second rank, as defined in the molecular frame of reference. The first term (the tensor part of the interaction) may be put into the same form as the direct spin-spin interaction, given in Eq. II(9), with a different interaction constant, c_3'', related to the d_{ij}. The sum of the direct spin-spin interaction constant, $c_3' = \frac{\mu_1\mu_2}{R^3}$, and the tensor part of the electron coupled spin-spin interaction constant, c_3'', is called the coupling constant for the tensor part of the spin-spin interaction, denoted by c_3. c_4 is called the scalar part of the spin-spin interaction, where its electron-coupled origin

is to be understood.

English (1966, Appendix B) has derived the matrix elements for the c_3 and c_4 interactions. These appear in Table II(2), where a Wigner 9-j symbol appears in the c_3 matrix element.

Theoretical and semiempirical formulas for c_3'' and c_4 can be found in (Ramsey, 1953) and (Schlier, 1961). These are extremely complicated and require much more information about the electronic structure of the molecule than is available in the case of molecules such as the thallium-halides. One point of interest, however, is that both c_3'' and c_4 are proportional to the product of the nuclear g-factors (note that c_3' also is proportional to this product). Since we have measured c_3 and c_4 in all four isotopic species of TlBr it will be possible to verify this proportionality (Chapter VI, Sec. V.B.3.)

The above interactions, the nuclear electric quadrupole interaction and the nuclear magnetic dipole interactions, make up the principal hyperfine interactions that have been observed in diatomic molecules such as the Tl-halides. Part of our task is to determine whether these interactions are sufficient to explain quantitatively the observed hyperfine spectrum to within the uncertainty of the measurements. For example, it may be necessary to include the magnetic octupole interaction of the Br nucleus to fit the observed spectrum. In Chapter V we shall discuss this problem in more detail.

II.C. Composite Hamiltonian and Matrix Elements

We will now write down the various terms of the interaction Hamiltonian which we have considered significant for the description of the hyperfine structure of a molecule such as TlBr in zero external fields:

$$H_{hfs} = \underbrace{F^{(2)} \cdot Q^{(2)}}_{\text{Quad. interaction}} \qquad \underbrace{c_1 \vec{I}_1 \cdot \vec{J} + c_2 \vec{I}_2 \cdot \vec{J}}_{\text{spin-rotation}}$$

$$+ c_3 \frac{2[3(\vec{I}_1 \cdot \vec{J})(\vec{I}_2 \cdot \vec{J}) - (\vec{I}_1 \cdot \vec{I}_2)(J(J+1)]}{(2J-3)(2J+3)}$$

tensor part of spin-spin

$$+ c_4 \vec{I}_1 \cdot \vec{I}_2$$

scalar part of spin-spin

where the symbols have been previously defined in the text.

Table II(2) shows the matrix elements of the above interactions, calculated in the coupled representation

$$|[\alpha(I_1 J)F_1 \; I_2]F \; M_F\rangle .$$

II.D. Energy Levels

The energy levels which result from the hyperfine interactions are best described with the aid of an energy level diagram. For illustration, let us consider the hfs in the J=1 rotational state of TlBr shown in Figure II(1).

The initial splittings of the J=1 rotational level are

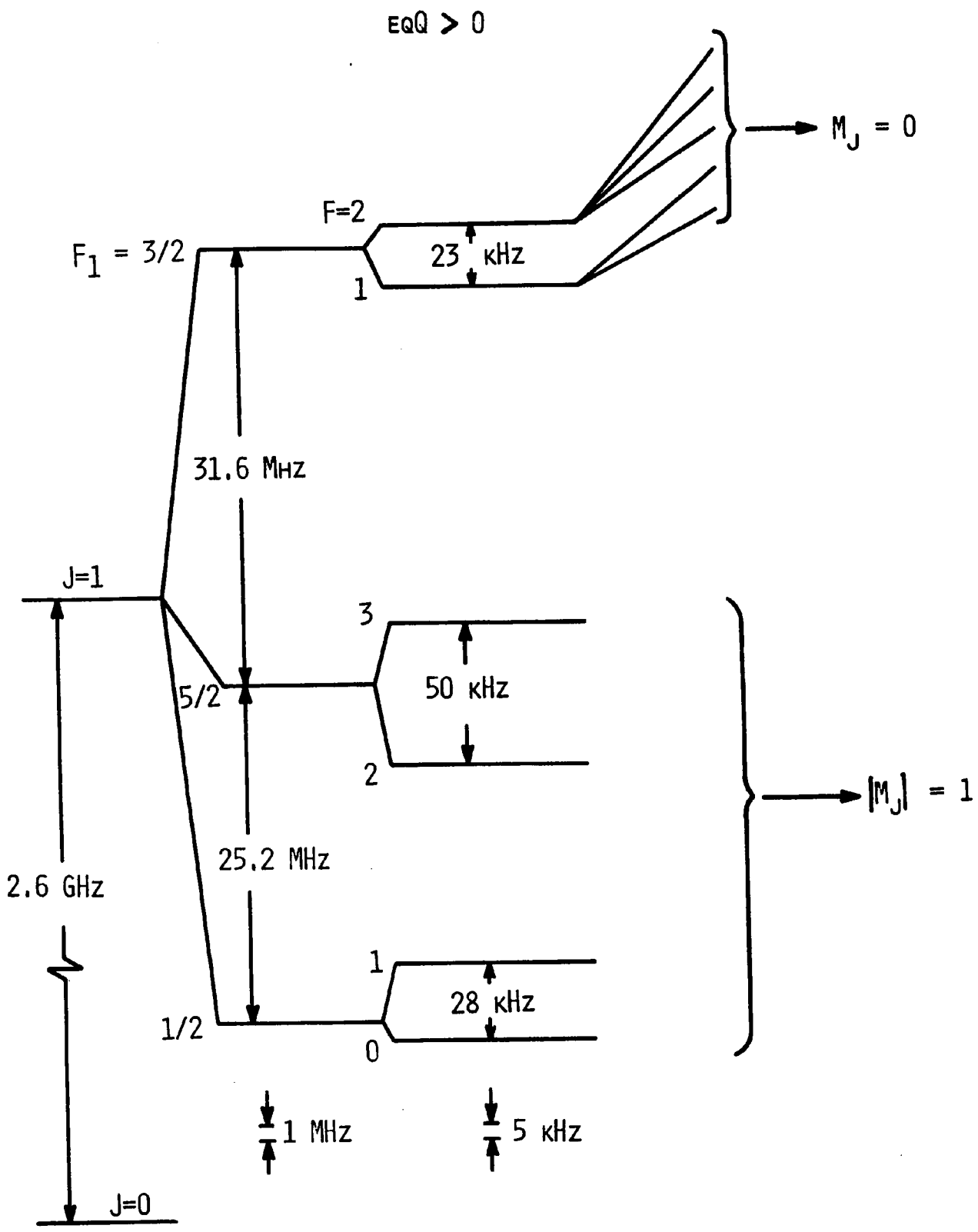


Figure II(1) J = 1 Energy Level Diagram of TlBr.

those labeled by F_1 and are due to the quadrupole interaction of the bromine nucleus (I = 3/2) plus the bromine spin-rotation interaction.

Table II(2). Matrix Elements of H_{hfs}

$$\langle[(JI_1)F_1,I_2]F,M_F|H_{hfs}|[(J'I_1)F_1',I_2]F,M_F\rangle$$

$$= \frac{eqQ}{4}(-1)^{I_1+J+J'+F_1}\delta_{F_1'F_1}\sqrt{(2J'+1)(2J+1)}\begin{Bmatrix} F_1 & J' & I_1 \\ 2 & I_1 & J \end{Bmatrix}\begin{pmatrix} J' & 2 & J \\ 0 & 0 & 0 \end{pmatrix}\begin{pmatrix} I_1 & 2 & I_1 \\ -I_1 & 0 & I_1 \end{pmatrix}$$

(quadrupole interaction at nucleus 1)

$$+c_1\left(\tfrac{1}{2}\right)\delta_{F_1'F_1}[F_1(F_1+1)-I_1(I_1+1)-J(J+1)]$$

(spin-rotation interaction at nucleus 1)

$$+c_2(-1)^{[J+I_1+2F_1'+I_2+F+1]}\left[J(J+1)(2J+1)NS_2\right]^{\frac{1}{2}}\begin{Bmatrix} F & I_2 & F_1 \\ 1 & F_1' & I_2 \end{Bmatrix}\begin{Bmatrix} J & F_1 & I_1 \\ F_1' & J & 1 \end{Bmatrix}$$

(spin-rotation interaction at nucleus 2)

$$+c_3(-1)^{[F_1'+I_2+F+1]}\left[\frac{30J(J+1)(2J+1)}{(2J+3)(2J-1)}\ NS_1S_2\right]^{\frac{1}{2}}\begin{Bmatrix} F & I_2 & F_1 \\ 1 & F_1' & I_2 \end{Bmatrix}\begin{Bmatrix} J & J & 2 \\ I_1 & I_1 & 1 \\ F_1 & F_1' & 1 \end{Bmatrix}$$

(tensor part of spin-spin interaction)

$$+c_4(-1)^{[J+I_1+F_1+F_1'+I_2+F+1]}(NS_1S_2)^{\frac{1}{2}}\begin{Bmatrix} F & I_2 & F_1 \\ 1 & F_1' & I_2 \end{Bmatrix}\begin{Bmatrix} J & I_1 & F_1 \\ 1 & F_1' & I_1 \end{Bmatrix}$$

(scalar part of spin-spin interaction)

where

$$N \equiv (2F_1+1)(2F_1'+1),$$

$$S_1 \equiv I_1(I_1+1)(2I_1+1),$$

$$S_2 \equiv I_2(I_2+1)(2I_2+1).$$

The $c_1\vec{I}_1\cdot\vec{J}$ interaction contributes only 4-10 kHz to the splittings compared to the tens of MHz from the much larger quadrupole interaction.

The further splittings, labeled by their F values, are due to the magnetic interactions involving the thallium nucleus (i.e., the c_2, c_3, and c_4 interactions). In Figure II(1) we have expanded the scale for successive splittings to show them more effectively. The magnitudes of the splittings given in the diagram are those for the ground vibrational state (v=0) of $^{205}Tl^{79}Br$.

II.E. Observability Criteria

A major factor determining the observability of a particular hyperfine transition is the focusing characteristics of the two energy levels in the MBER spectrometer. Each (F,M_F) hyperfine level in weak electric field corresponds adiabatically to an M_J level in strong field (where M_J is the projection of J along the direction of the electric field). Beam molecules in particular (J,M_J) states are focused onto the detector of our spectrometer by the strong, inhomogeneous electric focusing fields, while other (J,M_J) states are defocused. The weak field-strong field correspondence* for J=1 is symbolized in Figure II(1) by the array of lines to the right of the figure. In our spectrometer the J=1, M_J=0 states are focused, whereas the $|M_J|$=1 states are defocused.

*A discussion of the weak field-strong field adiabatic correspondence of the hyperfine states of a diatomic molecule has been presented by Hughes and Grabner (1950).

Consequently, in J = 1 of TlBr, only the two top F levels (of the $F_1 = 3/2$ level) correspond to focused states. A transition is observable in our spectrometer when it occurs between a focused state and an unfocused state. Hence for TlBr in the J = 1 rotational state, there are eight such observable transitions.

Other factors which sometimes reduce the number of transitions in the observed spectrum are selection rules. In our case, where transitions are induced in very weak electric and magnetic fields, the selection rules are (Hughes and Grabner, 1950):

$$\Delta F_1 = 0, \pm 1, \pm 2 \qquad \Delta F = 0, \pm 1, \pm 2$$

and $\Delta M_F = 0$ for $E_{rf} \parallel E_{dc}$

$\Delta M_F = \pm 1$ for $E_{rf} \perp E_{dc}$

where E_{rf} represents the oscillation radio-frequency electric field strength in the transition region, and E_{dc} represents the static or dc field strength in the transition region.

In our transition region there are components of E_{rf} both parallel and perpendicular to E_{dc}, so that ΔM_F may be taken as both 0 and ±1. Thus from the J = 1 energy level diagram it is seen that all of the lower F_1,F levels are connected to the upper two F levels by these ΔF_1, ΔF selection rules, implying that all eight observable transitions are also allowed.

II.F. Factors Determining Amplitudes of Observed Transitions

The amplitude of an observed transition depends both on the transition probability and on the populations of the involved hyperfine states in the beam passing through the transition region of the spectrometer. The transition probability itself vanishes for the single quantum hyperfine transitions which we are discussing in the case of zero external electric field. A static electric field is necessary in the transition region in order to induce a small effective electric dipole moment in the molecule (in zero field, the molecule's rotational motion averages the molecule's permanent electric dipole moment to zero). The presence of an electric field introduces undesired shifts and broadening of the observed resonances due to the Stark effect. Consequently, in making the measurements one attempts to compromise between the Stark effect and the signal-to-noise ratio.

The problem of actually calculating transition probabilities for the hyperfine transitions we are discussing and for the field strengths encountered in the transition region is one of great difficulty. Hughes and Grabner (1950) discuss the obstacles to a satisfactory solution to the problem.

An additional factor influencing the size of transitions is the population of the various F_1, F, M_F states in the beam as it passes through the transition region. This is determined by the total beam intensity, the effect of the focusing fields in their role as state selectors, and by the occurance of diabatic transitions out of the normally focused

states. The latter occur frequently when the molecules leave the first focusing field where the molecule passes rapidly from a strong field region into essentially a field-free region. Since such transitions alter the distribution of states of the molecules in the transition region, they can influence significantly the amplitudes of the observed transitions. In Chapter III we shall discuss further the effect of the focusing fields on the populations of hyperfine states.

CHAPTER III

APPARATUS

The molecular beam electric resonance spectrometer used to study the hyperfine structure of the Tl-halides was essentially the same instrument designed and constructed by Zorn and English, and is described in great detail by English (1966). Only a brief discussion of the apparatus will be given here, excepting modifications which will be presented in more detail.

Fig.III(1) shows a cutaway diagram of the apparatus. The essential features are (1) the oven, (2) the first 4-pole focusing field (the A-field), (3) the transition region (the C-field), (4) the second 4-pole focusing field (the B-field), and (5) the hot-wire detector. These items are mounted inside a vacuum enclosure as shown.

III.A. Oven Chamber, Oven Mount, and Oven

A major modification to the vacuum enclosure was the replacement of the oven chamber. The new oven chamber is essentially a square box constructed from brass and aluminum plates. The method of construction is described in Appendix C. The major advantage of the design is that all parts of the chamber are readily accessible, making it considerably easier

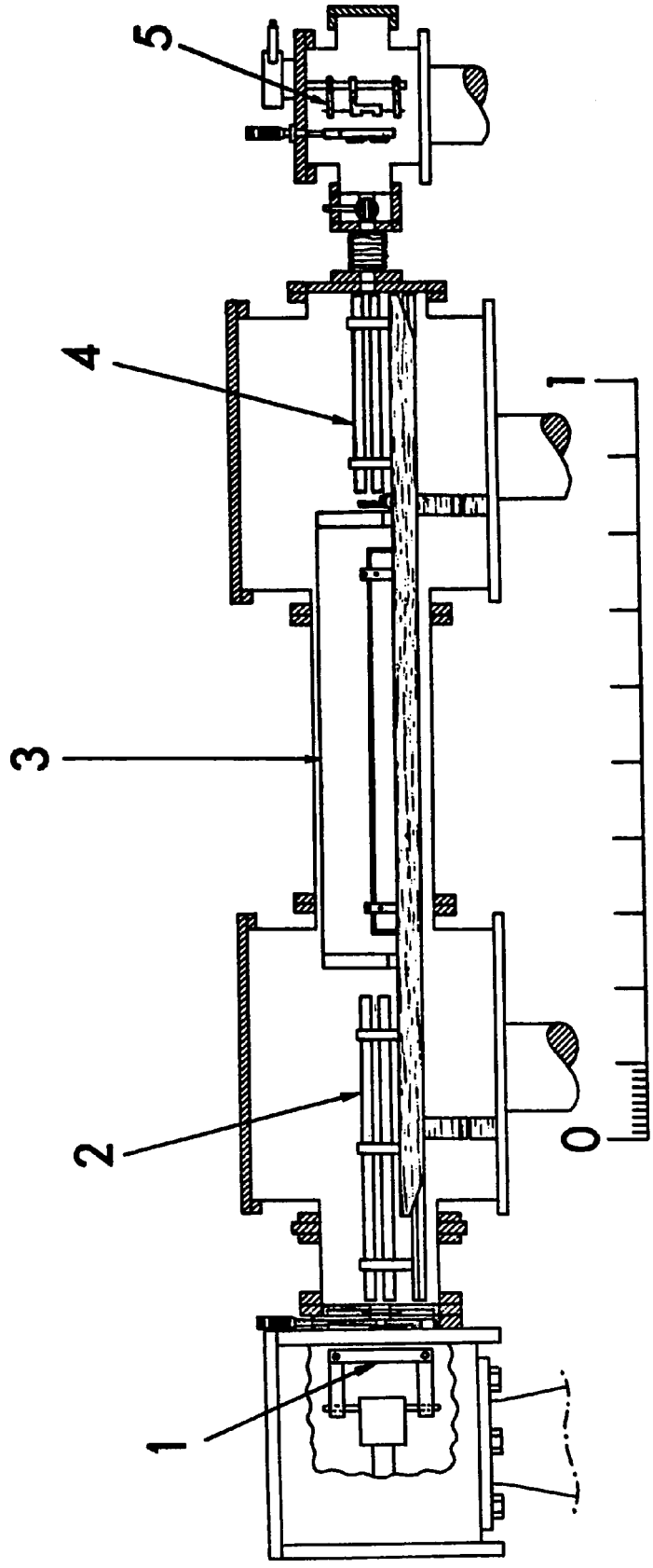
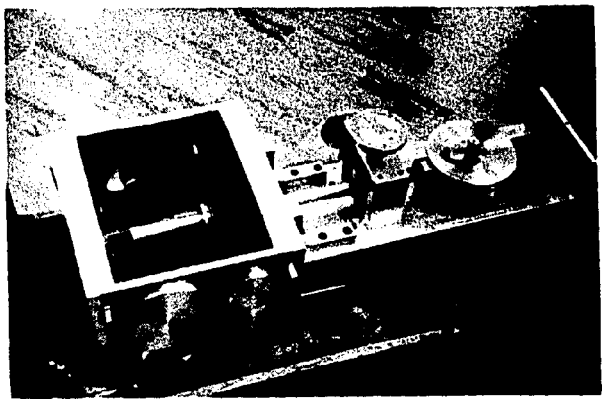


Figure III(1) Cutaway Diagram of Apparatus.

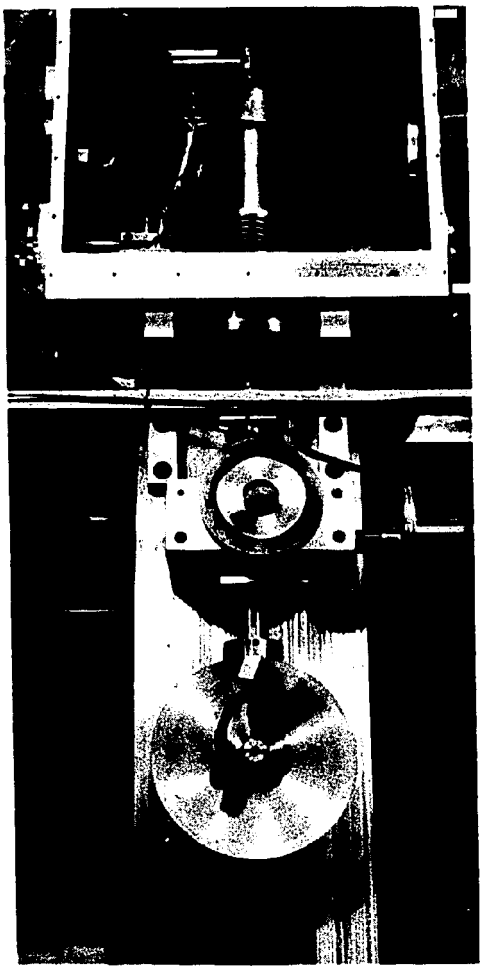
to install ovens, heat shields, thermocouples, etc. A copper chevron baffle sits on the inside of the oven chamber over the hole to the diffusion pump. This greatly reduces the back-streaming of diffusion pump oil up into the oven chamber. The chevron baffle and the front and back walls of the oven chamber are water cooled. The chamber is pumped with a NRC VHS6 2400 liter/sec diffusion pump which is capable of bringing down the pressure inside the chamber to 1×10^{-7} torr in less than three hours. To trap condensible vapors, a liquid nitrogen cold trap penetrates into the chamber through the lid.

Figure II(2) shows two views of the oven mount and oven chamber. The oven mount allows three dimensional movement of the oven by means of screws and levers that are external to the vacuum system. The design is a modification of an oven mount used on another molecular beam apparatus (Miller, 1966 1967). The modifications are primarily an enlargement of the components to provide greater mechanical stability, and a provision for retracting the oven mount along the beam axis. The latter feature permits the oven to be placed very close to the entrance of the first 4-pole focusing field, yet allows the oven to be easily installed and removed by retracting the oven mount one or two inches.

Fig. III(3)is a photograph of the oven in its installed position on the oven mount inside its chamber. The oven is a stainless steel tube with 0.005 in. wall thickness, $\frac{1}{2}$ in. O.D., and approximately $4\frac{1}{2}$ in. in length. A hole is made in the center of the tube by first cutting a 0.006 in. wide vertical slot which does not quite penetrate through the



(a) View of Oven Mount and Oven Chamber before Installation onto MBER Spectrometer.



(b) View of Oven System.

Figure III(2) Oven Mount and Oven Chamber.

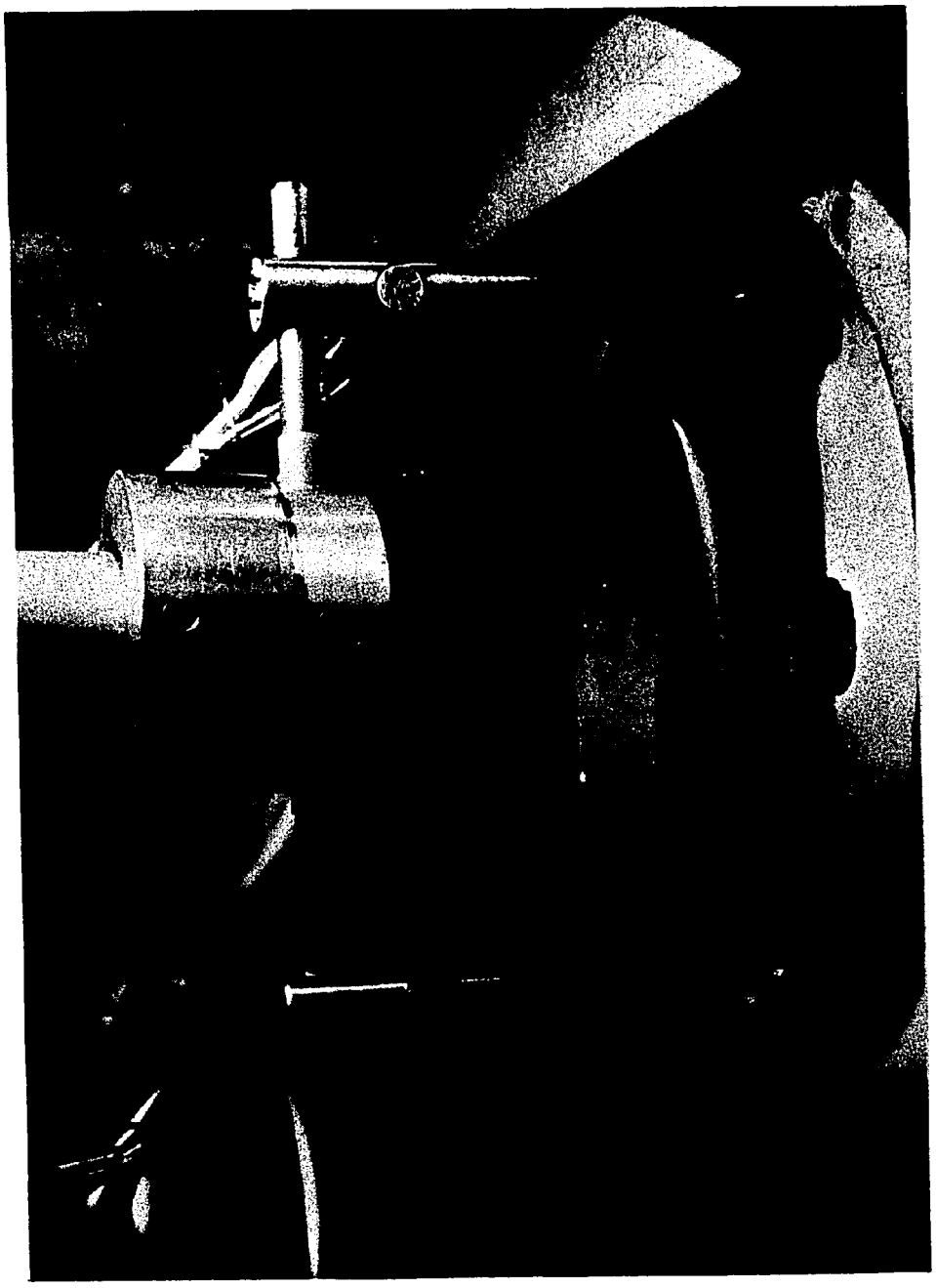


Figure III(3) Tube-Oven Installed in Oven-Holder, inside Oven Chamber.

tube wall. Then a tungsten wire 0.003 - 0.005 in. in diameter is pushed through the thinnest part of the slot. This procedure is simply a cheap way of producing a very small hole in the stainless steel tube wall. One end of the tube is crimped and folded twice in a vise. A charge of five to ten grams of the salt to be vaporized is placed inside the tube and the top is also crimped and folded twice. The tube-oven is then placed in the oven holder, as shown in the photograph, and clamped securely.

Large flexible cables are attached to the oven supports to carry the heating current which flows directly through the tube-oven. The current supply consists of a line regulator, a variable-voltage-transformer, and a heavy-duty step-down transformer. A typical heating current of 40 amperes with a voltage drop of about one volt across the secondary of the transformer heats the center part of the tube-oven to about 500° C when the oven is inside a vacuum.

III.B. Detector

The detection of TlBr, as well as the other thallium-halides, is accomplished by surface ionization of the molecule on an oxygenated tungsten wire. The wire is located in the detector chamber, approximately 1.5 meters from the oven. The positive ions produced on the surface of the wire are collected by a biased metal plate, producing a current which is measured with a sensitive vibrating-reed electrometer (Cary model 31, manufactured by Applied Physics Corp.). Oxygen, supplied by

a General Electric Silver Permeation Leak (model 22HL030) through a 1/8 in. copper tube, is sprayed onto the tungsten wire at a rate of about 4×10^{-3} micron liters/sec. The wire is simultaneously heated to about 1400° K by passing a direct current through it. The oxygen reacts with the hot tungsten surface to form a layer of tungsten oxide a few molecules in depth. This raises the work function of the surface from about 4.5 eV to about 6.2 eV. (The actual value of the work function obtained by oxygenation is very difficult to predict because it depends on conditions of the surface, such as the presence of impurities or the orientation of crystalline planes, all of which is unknown.) The ionization potential of atomic thallium is 6.106 eV (Moore, 1949). Consequently a thallium atom on the surface of the wire is likely to give up an electron to the surface, and the ion produced will be thermally kicked off the surface to be collected.

In our spectrometer it is desirable to have a detector wire which is about 0.015 in. in diameter because this is approximately the width of the focused image of the 0.004 in. oven aperture produced by the 4-pole focusing fields (yet to be discussed). Generally a wire of conventional commercial grade tungsten and of 15 mils in diameter would produce an intolerably large background ion current from impurities of alkali atoms in the wire. We have produced wires of this size, by a method described by Greene (1961), that are at least an order of magnitude quieter than commercial wire and have proved to make excellent detector wires in our spectrometer.

Basically they are made by depositing pure tungsten from a $W(CO)_6$ vapor onto a 0.003 substrate tungsten wire* which is heated to about 2400° C during the deposition. Since we have started with a relatively clean substrate of small diameter, the alkali impurities trapped inside the pure tungsten coating are far less than ordinary tungsten wire of the larger diameter. Some of the impurities appear to migrate to the pure tungsten surface to produce a background current. But the wire noise so produced is significantly smaller than fluctuations in the detected beam, and hence can be tolerated. For a more complete discussion of our methods of manufacturing these coated wires and of their use in the detection of the thallium-halides, see Stephenson (1968).

III.C. Focusing Fields

Several investigators have used 4-pole focusing fields for state selection in a beam of polar molecules [see Bennewitz (1955), English (1966), and Miller (1967)]. Fig.III(4) shows a drawing of one of the fields. It consists of four parallel rods arranged so their centers lie on the corners of a square. Two rods diagonal to each other are grounded, while the other two rods are raised to a high voltage, V, typically five to 20 kilovolts. This electrode geometry results in an inhomogeneous electric field whose absolute magnitude increases linearly with the radial

*This wire is extraordinarily free of alkali metal impurities and was obtained from General Electric.

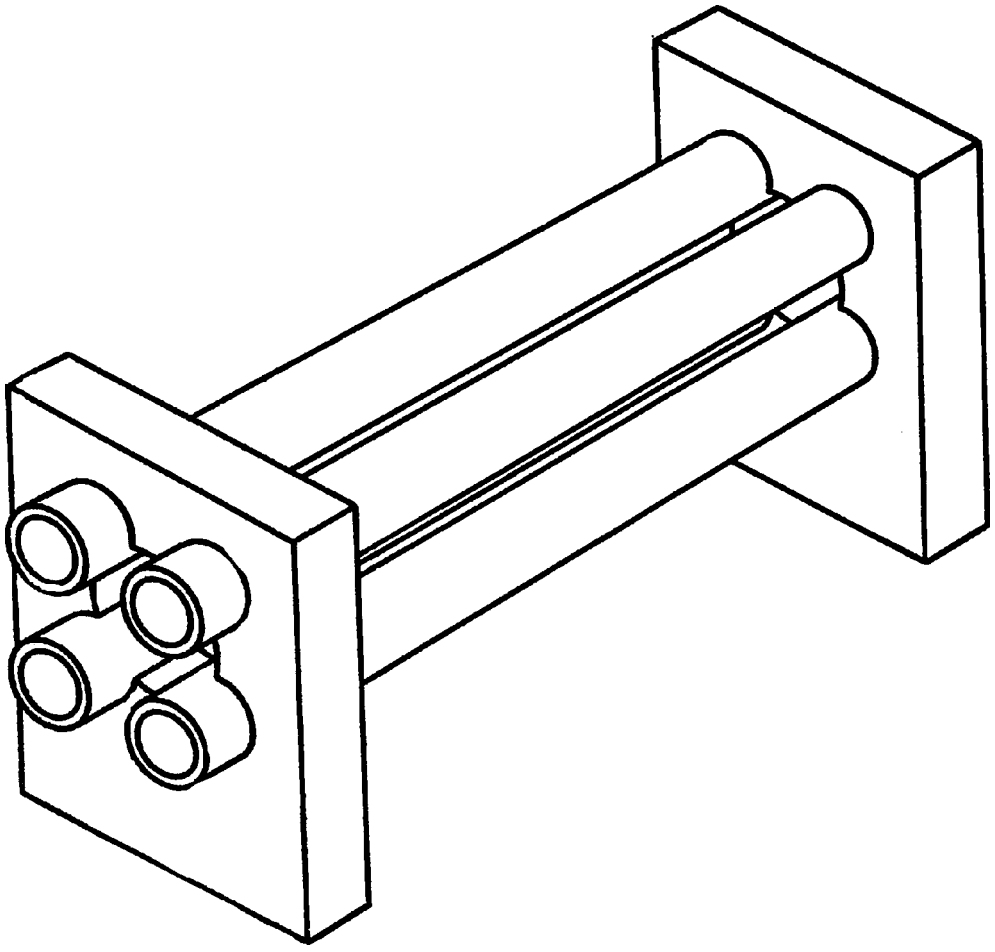


Figure III(4) 4-Pole Focusing Field.

distance from the axis. The trajectory of a polar molecule moving through the central region of such an electric field, with most of its velocity along the symmetry axis of the apparatus, is dependent upon its rotational angular momentum quantum number, J, and its spatial quantum number, M_J. Molecules in one set of (J, M_J) states experience a force away from the symmetry axis of the machine which is sufficiently strong so that these molecules miss the detector. Another set of (J, M_J) states are deflected significantly towards the symmetry axis and can therefore be focused onto the detector. Finally, a third set either undergo zero deflection or insignificant deflections and would be detected if we did not prevent them from hitting the detector. The last set of molecules are removed from the beam by placing a small obstacle directly on the symmetry axis of the machine. In our case this obstacle, called the center-stop, is located at the entrance to the B-focusing field. The center-stop casts a shadow in the beam, completely masking the detector from any molecule which leaves the oven aperture and travels in a straight line. Yet the center-stop is small enough so that the molecules in the second, focused set can be deflected around it onto the detector. With the center-stop in place and no voltage applied to the A and B fields there is always a small background of detected beam molecules, caused by the random scattering of beam molecules by the residual gas molecules. Since this background contributes only to the noise and not to the signal, it is advantageous to minimize it by maintaining sufficiently good vacuum along

the beam path. Experience with this machine has shown that an operating pressure near 1×10^{-7} torr from the entrance to the A-field to the detector is necessary for a good signal-to-noise ratio.

In Appendix B an expression [Eq. B(13)] is derived to determine the voltage, V, to apply to the focusing fields in order to focus a particular J, M_J state onto the detector. In Appendix C, an analysis of the effective aperture of the focusing fields is presented for each focusable (J, M_J) state. It is shown how this affects the number of (J, M_J) molecules which reach the detector, and therefore the amplitudes of the observed transitions. In particular it explains why transitions in the J = 1 hfs of TlBr were so difficult to observe.

Because of the inability to focus an adequate number of J = 1 molecules, careful measurements of TlBr hfs were limited to the J = 2 and J = 3 rotational states. The voltage necessary to focus J = 4, M_J = 0 is predicted to be 17.3 kV. Our focusing fields would hold only about 14 kV, where there appeared only slight indications of signal for J = 4 transitions. It was not considered worth the effort and cost to build focusing fields to maintain higher voltages.

III.D. Transition Region

Transitions between the various hyperfine levels are induced in the transition region, or C-field. The C-field in

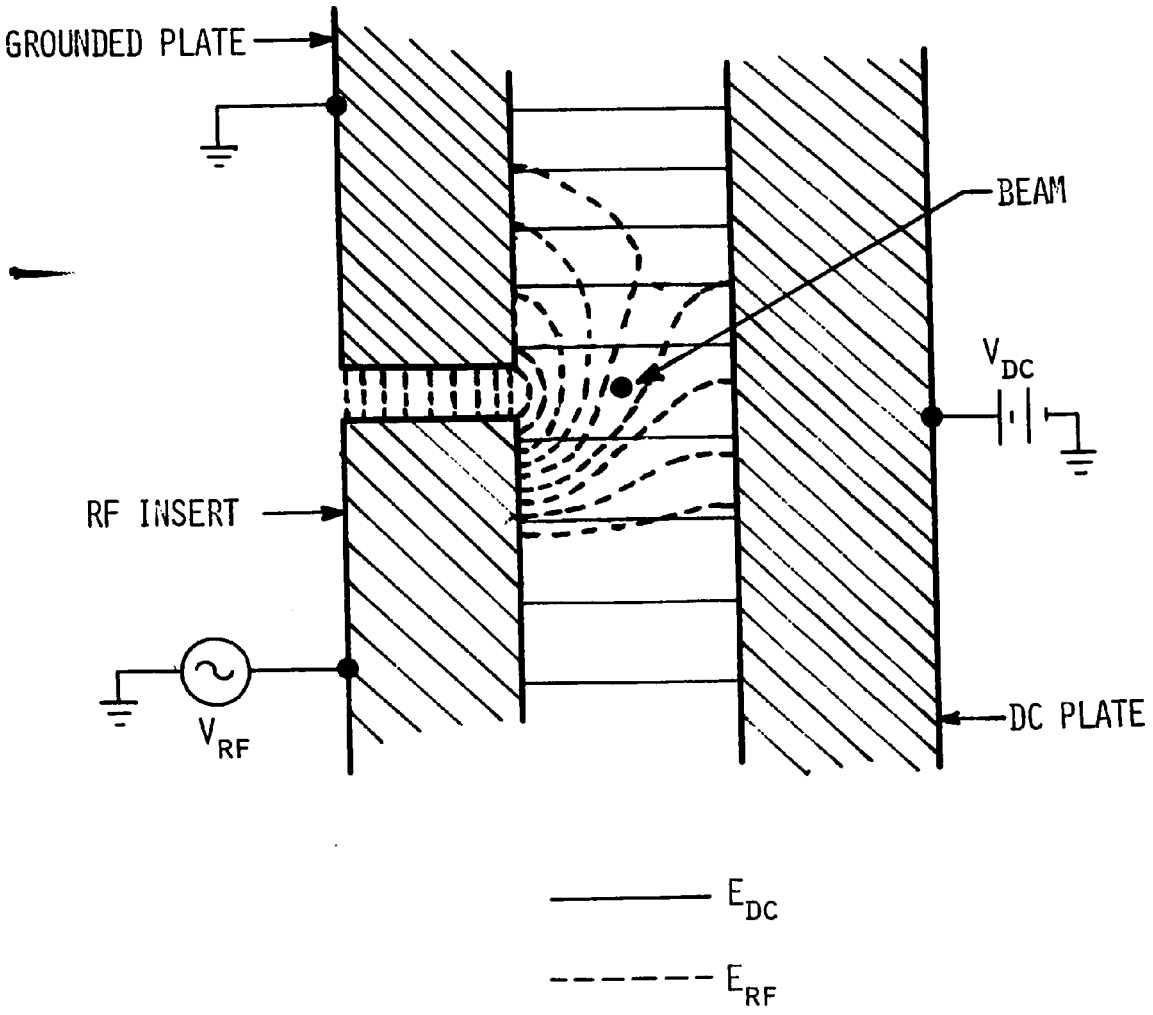


Figure III(5) View of C-Field Electrodes with Approximations to the Electric Field Lines Indicated.

our apparatus is described by English (1966, p. 111). It is a modified Trischka design (Marple and Trischka, 1956) consisting of two parallel aluminum plates separated by 1 cm quartz spacers. One of the plates contains a 51 cm long insert insulated and supported from its surrounding plate. A radio-frequency voltage is applied to the 51 cm insert, with its surrounding plate grounded. The opposite plate is raised to a small constant potential with respect to ground. In Figure III(5) are shown the electrodes in the region where the beam passes. Also indicated are rough estimates of the electric field lines, both for the rf and the dc fields.

Marple and Trischka have analyzed quantitatively the electric fields inside a field of the Trischka design. Following their arguments we may estimate the field strengths in the region where the beam passes. These are found to be:

$$E_{rf_{\parallel}} = 0.64 \ V_{rf} \text{ volts rms/cm}$$

$$E_{rf_{\perp}} = 0.20 \ V_{rf} \text{ volts rms/cm}$$

where $\parallel$ and $\perp$ refer to the components of the rf field parallel and perpendicular to the dc electric field, respectively, and V_{rf} is the applied rf voltage. The dc field strength is equal to the voltage applied divided by the separation between the field plates (1.0 cm). Typically, $E_{dc} = 1.5$ V/cm.

Ramsey (1956, p. 123) gives the following formula for the line width of a transition in a two level system observed in a molecular beam spectrometer (i.e., full width at half

maximum of the transition probability averaged over the velocity of beam):

$$\nu(\text{kHz}) = [1.072\ \alpha(\text{cm/sec})]/[10^3\ L(\text{cm})] \qquad \text{III(1)}$$

where L is the length of the transition region, and α is the most probable molecular velocity inside the source, given by

$$\alpha = \sqrt{2kT/m} \qquad \text{III(2)}$$

where k = Boltzmann's constant, T = oven temperature in °Kelvin, m = mass of the molecule. We obtain a value for $\alpha = 2.0 \times 10^4$ cm/sec where T is taken to be 750° K and m = 284 amu (the mass of TlBr). For a transition region of 51 cm length, we obtain a predicted line width of 415 Hz. This is in reasonably good agreement with the narrowest experimentally observed line width of 450 Hz. Better agreement is not really expected because, first, the focusing fields distort considerably the velocity distribution of the beam molecules so that the average over ν is very likely altered, and second, the hyperfine energy levels involved in the transitions do not make up a simple two level system (e.g., the 2F+1 degeneracy in M_F of each F level). Nevertheless, Eq. III(1) and III(2) have been compared with experimentally observed line widths in our spectrometer on several combinations of molecules, oven temperature, and C-field length, and the agreement has always been better than 20%.

The rf voltage is fed to the 51 cm insert by means of coaxial cable which penetrates the vacuum envelope by means of a vacuum tight General Radio type N connector. The coax

inside the vacuum is Amphenol RG 140/U which has a teflon dielectric. The outer insulated coating has been removed to expose the braided shielding for quicker outgassing. The rf voltage is applied at one end of the insert, while the other end is terminated to ground with a 50 ohm resistor. Since this geometry could permit traveling waves to occur, the question arose of their effect on the measured resonance. As Ramsey (1956) points out, a traveling wave in one direction of the transition region will lead to a shift in the line position due to the Doppler effect. If the wave travels in the opposite direction to the motion of the beam molecules the shift in the measured line center will be down in frequency from the real line center. The magnitude of the shift is given by:

$$\Delta\nu_{\text{Doppler}} = \nu\, v/c$$

where ν = transition frequency
v = beam velocity
c = velocity of light

The highest frequency lines observed in TlBr are in the 54 MHz region. With an average beam velocity of 2.6×10^4 cm/sec (1.33 α), the Doppler shift would be about 50 Hz in this high frequency region. A test for such a shift was carried out, wherein a 54 MHz line was observed with the feed and termination of the insert in one direction, then reversed. The two lines were compared at all points very carefully, with no visible shift or change in line shape observed. It is estimated that such a comparison would be able to detect any shift larger than 25 Hz, so there was no

need for correcting the measured frequencies for the Doppler effect.

The sources of radio-frequency voltage supplied to the transition field is a Hewlett-Packard 606 B Signal Generator with frequency stabilization provided by a Hewlett-Packard 8708 A Synchronizer. The unit has a frequency stability of about five parts in 10^8 over a period of ten minutes. The frequency can be set to one part in 10^7 with no difficulty. The frequency of the generator's output is measured with a Hewlett-Packard 5245 L Electronic Counter calibrated to a few parts in 10^9 in terms of the VLF signal from the Boulder Laboratory of the National Bureau of Standards. Hence, in principle, the frequency measurements can easily be made to better than one thousandth of a line-width, where in practice, one hundredth of a line-width is entirely sufficient for this experiment.

III.E. Data-taking System

A hyperfine transition is detected with the spectrometer when the induced transition produces a change in beam intensity that is sufficiently large compared to the combined beam and detector noise. A change in beam intensity will occur when the transition is between a focused hyperfine level and one which is defocused. One can increase the signal to noise ratio considerably by measuring the change in beam intensity as a function of frequency while the radio frequency voltage is alternately applied and removed from the C-field.

Further improvement is obtained by repeating the measurement at a given frequency several times and averaging the resulting changes in intensity. Since the noise is practically all random, the signal-to-noise ratio is expected to increase as $\sqrt{N}$ where N is the number of readings taken at each frequency. This expectation is fulfilled experimentally. For the measurements on TlBr, an acceptable signal-to-noise ratio was generally achieved with N = 10. For some of the weaker transitions as many as 50 readings per frequency were taken.

The semi-automatic system used to take the data consists of the following components:

1. A motor-driven, programmable switching array to provide gating pulses, reset commands, etc.

2. A Dymec 2401 C Integrating Digital Voltmeter, which can be gated, reset, and have its polarity reversed. This instrument reads the output of the Vibrating-Reed Electrometer in phase with the RF on- RF off-cycle so as to measure the change in detected beam current. The Voltmeter is gated for precisely one second and integrates the electrometer output over this time.

3. A Hewlett-Packard 5245 L Electronic Counter to read the frequency of the Signal Generator.

4. A Hewlett-Packard 560AR Digital Printer which records on paper tape the change in beam intensity as measured by the Voltmeter, and the frequency as measured by the Electronic Counter.

5. A "frequency stepper," which is a device that supplies

a series of voltages in uniform steps that change the frequency of the signal generator when supplied to the external frequency modulation input of the synchronizer. The stepper can be set up to scan over the region of a transition, automatically stopping at predetermined intervals for N cycles of rf on- rf off.

Typically, 100 Hz steps are taken over a region 2 kHz wide. The recorded voltmeter readings are averaged by the operator and plotted as a function of frequency. A typical line taken in this fashion is shown in Fig. IV(3). Occasionally large noise spikes occur in the detected beam, usually caused by sudden increases in pressure inside the vacuum system or by violent action inside the oven. These pressure spikes and oven bursts occur typically once every ten minutes. Any data taken during these events are meaningless. For this reason, the detected beam current is monitored with a Varian G-10 Chart Recorder. When the operator sees an eruption in the beam, he can throw out the voltmeter readings that are affected.

III.F. Helmholtz Coils

In order to avoid the consequences of the splitting of the hyperfine levels due to the Zeeman effect, we have reduced the magnitude of the magnetic field in the transition region below where the effect influenced our results. This is accomplished by three sets of rectangular Helmholtz coils which surround the apparatus and are mounted orthogonally. The current in these coils is adjusted until the magnetic

field in the transition region is a minimum. The field is measured with a Bell Model 120 Hall effect gaussmeter. With the above coils we are able to reduce and maintain the magnetic field in the region of the C-field below 50 milligauss, which is sufficiently small that the Zeeman effect may be ignored in the analysis of the hfs spectra.

III.G. Operating Conditions

Table III(1) lists the important dimensions and typical operating conditions for the spectrometer.

Table III(1)
Operating Conditions

OVEN:			
	Aperture	0.004	in
	Volume	15	cc
	Charge of TlBr	5-10	gm
	Running time for one oven load	100	hr
	Applied voltage	0.9	volts
	Current	40	amps
	Temperature	750	°K
FOCUSING FIELDS:			
	Length of A-field	40.6	cm
	Length of B-field	26.0	cm
	Electrode diameter	1.6	cm
	Electrode spacing, R_o	0.64	cm
	Optimum voltage to focus J, $M_J = 0$ J = 1	5	kV
	J = 2	9	kV
	J = 3	13.5	kV
TRANSITION REGION (high resolution field):			
	Length	51	cm
	Spacing	1	cm

TRANSITION REGION (high resolution field):		
Applied rf voltage	2.0	volts rms
Applied dc voltage	1.5	volts dc
Line width	400-500	Hz
Magnetic field	50	milligauss
DETECTOR:		
Wire diameter	0.015	in.
Wire current	1.7	amp
Wire temperature	1500	°C
Oxygen leak rate	4×10^{-3}	micron-liter/sec
Collector bias voltage	22.5	volts dc
Total background current	1.5×10^{-12}	amps
Fluctuations in total background current (wire noise)	2×10^{-15}	amp
PRESSURE IN VACUUM SYSTEM:		
Oven Chamber	1×10^{-7}	torr
ABC Chambers	1×10^{-7}	torr
Detector Chamber	2×10^{-7}	torr
PERFORMANCE WITH TlBr:		
Detector efficiency (estimated)	40-90%	
Total Beam (center-stop out)	3×10^{-11}	amps
Scattered beam (center-stop in)	3×10^{-13}	amps
Refocused beam (center-stop in)	2×10^{-12}	amps
Beam fluctuations	5×10^{-15}	amps
Typical signal (change in beam intensity) for a J = 2, v = 0 spectral line in ^{205}TlBr	1×10^{-13}	amps

CHAPTER IV

RESULTS

IV.A. Search Work and Preliminary Measurements

IV.A.1. Low Resolution Search

From the results of Fitzky's microwave studies on TlBr (Fitzky, 1958) we were able to predict the frequencies of the hyperfine transitions to within ± 1 MHz. We used a 10 cm C-field to search over the regions where transitions were predicted. The line width for transitions in TlBr with this C-field is 5 kHz. During the search work, field intensities of 6 volts/cm dc and 2 volts rms/cm rf were employed.

Approximately fifty lines were observed at low resolution to make clear the line assignments as to J, v, (F_1,F), (F_1',F'), and isotope. All of the observed lines were accounted for by the predicted spectra of the J = 2 and J = 3 rotational states in the isotopes $Tl^{79}Br$ and $Tl^{81}Br$. The assignment as to thallium isotope was as yet uncertain. The entire frequency range covering the uncertainties quoted by Fitzky for his values of eqQ was searched in two different line groups with an eye toward finding the transitions due to the ^{203}Tl isotopic species. In addition, a similar search was made for transitions in the J = 1 hfs. The results of both searches were negative.

IV.A.2. High Resolution; the Two Thallium Isotopes

All lines were remeasured at high resolution using the 51 cm C-field with a line width of about 500 Hz. Most of the lines measured at this high resolution showed asymmetries or splittings. These splittings could not be explained by Stark or Zeeman effects because they were found to be independent of field strengths. Figure IV(1) shows the largest of the splittings that occurs in the J = 2, v = 0 hyperfine spectrum: The same transition for both bromine isotopes is shown. Since the observed line shapes in all cases could be matched with two superimposed lines of relative amplitudes 70:30, it was strongly suspected that we were observing the partially separated spectra of the two isotopes of thallium.

Further support for this hypothesis is provided by considering the properties of the thallium nucleus and of the molecule which could contribute significantly to the changes in hyperfine energy:

1. The nuclear magnetic moments of the two thallium nuclei differ by about 1%. Since c_2, c_3, and c_4 are all proportional to μ_{Tl}, this $\Delta\mu_{Tl}$ between isotopes will produce a change in the hfs. c_2 is by far the largest of the magnetic interactions in TlBr so that Δc_2 produces the largest contribution to Δf, the change in transition frequency, due to $\Delta\mu_{Tl}$. For example, in the (5/2,2) → (3/2,2) transition (λ_4) in $Tl^{79}Br$, v = 0, illustrated in Figure IV(1), Δf due to Δc_2 is predicted to be 700 Hz.

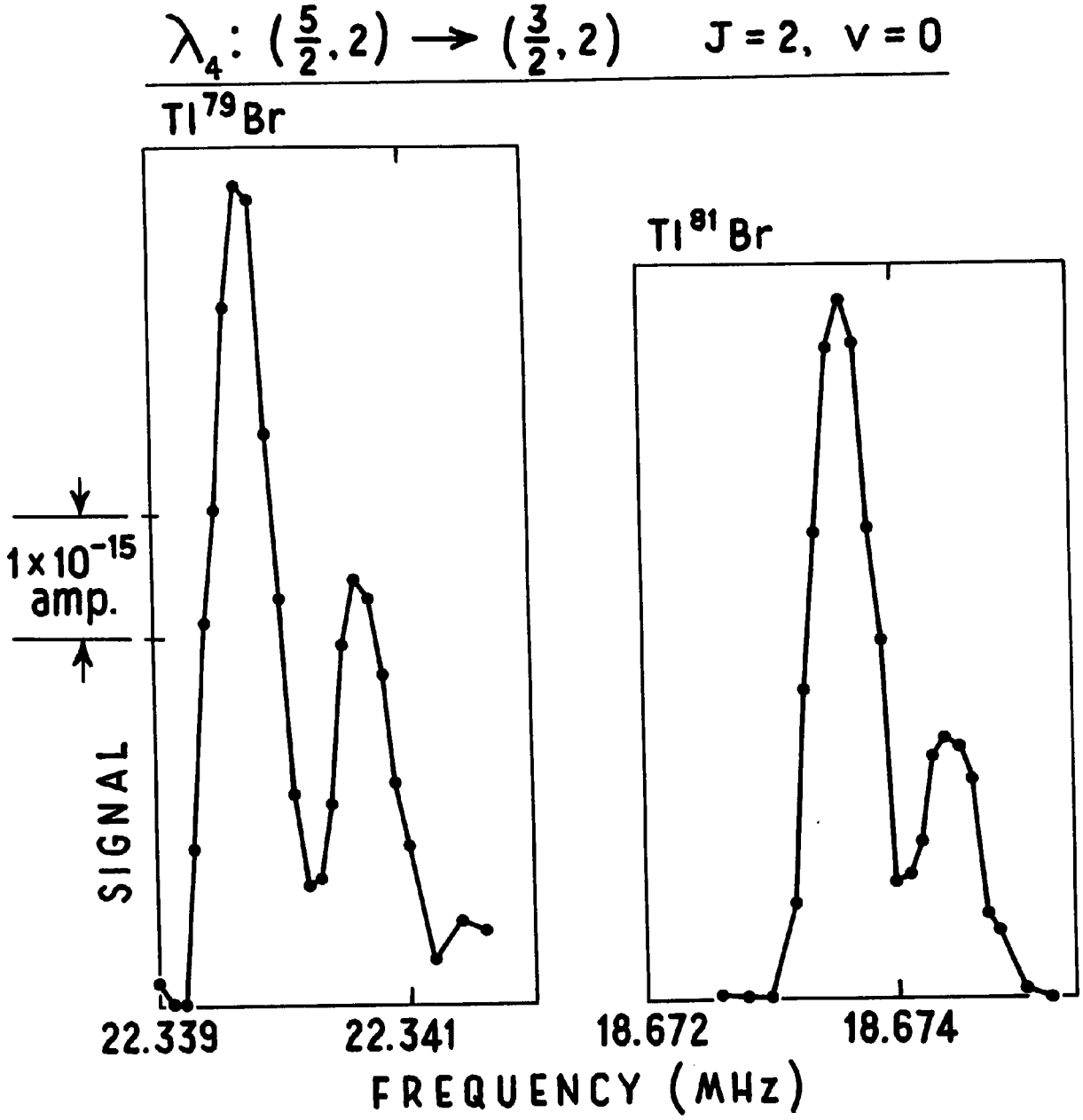


Figure IV(1) (5/2,2) → (3/2,2) Transition (λ_4) in J = 2, v = 0, TlBr.

2. The rotational constant of the molecule, B_v, changes by about .3% between ^{205}TlBr and ^{203}TlBr. This slightly changes the bromine quadrupole interaction energies between the two isotopic species because the second order quadrupole correction is proportional to eqQ^2/B_v. For example, the predicted Δf due to ΔB_v in the λ_4 transition is equal to 430 Hz.

The observed splittings agree quite well with those predicted from $\Delta\mu_{Tl}$ and ΔB_v. For example, in the λ_4 transition Δf is predicted to be 1130 Hz and it is observed to be 950 Hz. We are thus convinced that the two thallium-isotope hypothesis is correct.

IV.A.3. J = 1 Spectra

The analysis of the J = 2 and J = 3 spectra showed that the calculated constants for each J state predicted the line positions of the other J state to within ± 200 Hz. Consequently, it was safe to assume that the line centers for J = 1 transitions could be accurately predicted from J = 2 constants. After repeated searching under ideal conditions of signal to noise, a few J = 1 transitions were observed. The signals were so small that they were only useful for confirming that the J = 1 spectral lines were indeed in the expected place.

The J = 1 transitions are very weak because the effective aperture of the focusing fields for J = 1, M_J = 0 TlBr molecules is very small. This problem is discussed in detail in Appendix C.

IV.B. Determining Line Assignments

The task of determining line assignments for the observed spectra in TlBr is carried out with the help of a few basic characteristics of such spectra which we shall list here.

1. The lines appear in groups whose positions are determined primarily by the quadrupole interaction. If the line group is isolated and an approximate value of eqQ is known (as from Fitzky's work in the case of TlBr), then J can be easily determined. When line groups of different J overlap, they can sometimes be differentiated by plotting the intensity of the lines as a function of focusing voltage. Also, the magnetic interactions often produce discernable differences in the patterns of the line groups for different J which help to distinguish them.

A knowledge of J and a rough value of eqQ immediately allow us to assign F_1, F_1' to the line group.

2. The lines of a particular hyperfine transition in different vibrational states of the molecule are very nearly equally spaced due to a nearly linear change in eqQ with v. The ratio of line intensities between adjacent vibrational states is proportional to the thermal populations of the vibrational states in the beam, so that

$$I_{v+1}/I_v = e^{-\omega_e/kT} \qquad \text{IV(1)}$$

where I_v is the intensity of a particular hyperfine transition in the vth vibrational state, and I_{v+1} is the intensity of the corresponding transition in the v+1 vibrational state.

These two facts generally make line assignments with respect to v reasonably straightforward.

3. The values of F and F′ to be assigned to each line require a knowledge of the relative sizes and signs of the hyperfine constants c_2, c_3, and c_4. In many diatomic molecules the c_2 interaction dominates the spin-spin interaction. If we assume that c_2 is relatively large and also positive (c_2 is positive for all but the lightest diatomic molecules; see Sec. V.B.), the assignment of F,F′ is clear for the transitions which depend strongly on c_2. This initial assignment serves as a working hypothesis for obtaining a rough value of c_2, which assists in determining the F,F′ of the remaining lines of the group. In the TlBr J = 2 spectra, the c_2 interaction was much larger than the spin-spin interaction, allowing the F,F′ assignments to be made quite easily.

4. Because I_1 and I_2 are the same for all four isotopic species of TlBr, the same transitions are seen in all the isotopes and the line groups are nearly identical in structure. Hence, a one-to-one correspondence between the lines of the different isotopes is not difficult to establish. Such a correspondence often aids in determining line assignments for some of the isotopes when different vibrational states or rotational states have overlapping line groups.

IV.C. High Resolution Measurements

Hyperfine transition frequencies were measured at high resolution in the first five vibrational states and J = 2 rotational state for all four isotopic species of TlBr.

Approximately 160 J = 2 transitions were measured. Table IV(1) lists these observed frequencies and their corresponding line assignments. Intensities are listed for the $^{205}Tl^{79}Br$ J = 2, v = 0 spectrum normalized with respect to the most intense line in the spectrum, the (5/2,3) → (7/2,4) transition. This transition produced a change in beam intensity of approximately 3×10^{-14} amperes, with

$$V_{rf} = 2.0 \text{ v rms } (E_{rf} = 1.3 \text{ v rms/cm}) \text{ and } E_{dc} = 1.5 \text{ v/cm.}$$

A comparison of the relative intensities between the spectral lines is only approximate because the transitions were observed over an extended period of time with slightly different beam intensities.

A few J = 3 transitions were observed in the ground vibrational state and their frequencies are listed in Table IV(2).

The centers of the unresolved line-pairs corresponding to the two thallium isotopes were determined by a folding-out process. This consisted of taking an assumed ideal line shape obtained from the resolved lines of Figure IV(1), and superimposing two such lines with relative amplitudes of 70:30, with separated line centers of 100 Hz, 200 Hz, etc. The superimposed lines were then compared with the measured transitions, each properly normalized, and the superposition which matched the given line most completely was used to establish the line centers of the two components. Since the shape of the larger of the two components is affected less by the presence of the smaller, the uncertainties in the line centers are less for the larger components. An estimate of the uncertainties

TABLE IV(1)

TlBr HYPERFINE TRANSITION FREQUENCIES: J=2

$(F_1, F) \longrightarrow (F_1', F')$		
(2.5, 2)	(0.5, 0)	α_1
(2.5, 3)	(0.5, 1)	α_2
(2.5, 2)	(0.5, 1)	α_3
(2.5, 3)	(3.5, 3)	β_1
(2.5, 2)	(3.5, 3)	β_2
(2.5, 3)	(3.5, 4)	β_3
(2.5, 2)	(3.5, 4)	β_4
(2.5, 3)	(1.5, 1)	λ_1
(2.5, 3)	(1.5, 2)	λ_2
(2.5, 2)	(1.5, 1)	λ_3
(2.5, 2)	(1.5, 2)	λ_4

J=2, v=0

	$^{205}Tl^{79}Br$	$^{203}Tl^{79}Br$	$^{205}Tl^{81}Br$	$^{203}Tl^{81}Br$
α_1	54148.625	54148.625	45245.975	45245.975
α_2	54128.575	54128.500	45224.725	45224.725
α_3	54053.525	54054.125	45151.625	45152.200
β_1	31667.600	31667.150	26459.200	26458.800
β_2	31592.575	31592.575	26385.925	26385.925
β_3	31582.325	31582.325	26376.500	26376.500
β_4	31507.350	31507.700	26303.400	26303.900
λ_1	22483.000	22483.000	18813.650	18813.650
λ_2	22414.700	22415.100	18746.800	18746.800
λ_3	22408.100	22408.500	18740.725	18741.050
λ_4	22339.750	22340.700	18673.600	18674.400

J=2, v=1

α_1	—	—	45422.200	45422.200
α_2	54341.375	54341.775	45401.075	45401.200
α_3	54266.600	54267.450	45328.150	45329.000
β_1	31792.050	31791.500	26562.000	26561.700
β_2	31717.200	31717.275	26489.125	26489.125
β_3	31707.000	31707.100	26479.750	26479.750
β_4	31632.200	31632.700	26406.850	26407.400
λ_1	22569.950	22569.825	18885.900	18885.900
λ_2	22501.800	22502.375	18819.100	18819.400
λ_3	22495.200	22495.700	18813.075	18813.400
λ_4	22427.025	22428.025	18746.125	18747.025

J=2, v=2

	$^{205}Tl^{79}Br$	$^{203}Tl^{79}Br$	$^{205}Tl^{81}Br$	$^{203}Tl^{81}Br$
α_1	—	—	—	—
α_2	54552.875	54553.475	45576.150	45576.850
α_3	54478.350	54479.200	45503.500	45504.475
β_1	31915.700	31915.250	26664.350	26664.150
β_2	31841.075	31841.200	26591.700	26591.800
β_3	31830.900	31831.100	26582.325	26582.325
β_4	31756.300	31757.000	26509.650	26509.850
λ_1	22656.225	22656.450	18957.500	18957.750
λ_2	22588.300	22588.900	18890.850	18891.450
λ_3	22581.700	22582.350	18884.975	18885.400
λ_4	22513.775	22514.900	18818.225	18819.225

J=2, v=3

α_1	—	—	—	—
α_2	54763.000	54763.800	45750.200	45750.950
α_3	—	—	—	—
β_1	32038.550	32038.200	26776.100	26766.000
β_2	31964.100	31964.275	26693.475	26693.875
β_3	31953.950	31954.300	26684.200	26684.700
β_4	—	—	—	—
λ_1	—	—	—	—
λ_2	22674.225	22674.950	18962.100	18962.850
λ_3	—	—	18956.375	18957.100
λ_4	—	—	18889.825	18890.500

J=2, v=4

α_1	—	—	—	—
α_2	—	—	—	—
α_3	—	—	—	—
β_1	32160.750	32160.600	26867.100	26867.100
β_2	—	—	26794.750	26795.200
β_3	32076.275	32076.825	26785.425	26786.000
β_4	—	—	—	—
λ_1	—	—	—	—
λ_2	—	—	—	—
λ_3	—	—	—	—
λ_4	—	—	—	—

TABLE IV(2)

TlBr HYPERFINE TRANSITION FREQUENCIES: J=3

J=3, v=0

$(F_1,$	$F)\longrightarrow(F_1',$	$F')$		$Tl^{79}Br$	$Tl^{81}Br$
3.5	3.0	1.5	1.0	46306.600	—
3.5	4.0	1.5	2.0	46284.075	38675.100
2.5	3.0	1.5	1.0	31778.150	—
3.5	3.0	4.5	4.0	31576.775	26372.700
3.5	4.0	4.5	5.0	31571.600	26368.300
3.5	3.0	2.5	2.0	14654.800	12258.275
3.5	4.0	2.5	3.0	14653.650	12256.425

in the line centers obtained by this procedure are ± 50 Hz for the larger components (^{205}Tl) and ± 100 Hz for the smaller components (^{203}Tl). For the weakest lines, say those of higher vibrational states, these uncertainties are probably three or four times larger.

The observed J = 2 spectra for a particular v and isotopic species are explained with the aid of the energy level diagram shown in Figure IV(2). The strongest transitions observed are those which come out of the two top F levels of the $F_1 = 5/2$ level. This is to be expected since these are the only levels having M_F components which correspond to the strongly focused J = 2, $M_J = 0$ state in strong electric field. All of the allowed transitions out of the $F_1 = 5/2$ levels, eleven in number, were observed. The transition (5/2,3) → (7/2,4) is forbidden by the F selection rule. A few M_F sublevels of the $F_1 = 3/2$ hyperfine levels correspond in high field to the J = 2, $|M_J| = 1$ state. However, the focusing field aperture for this state is considerably smaller than for J = 2, $M_J = 0$ (see Appendix C), so that transitions out of the $F_1 = 3/2$ levels are expected to be weak. Experimentally, these transitions were indeed small, with a signal-to-noise so poor that the line centers could not be chosen to less than ± 400 Hz. Consequently they were not used in the calculation of the constants.

Figure IV(3) shows the J = 3 hfs diagram and illustrates the correspondence to the high field states. The J = 3 states which are strongly focused are the two top F levels of the

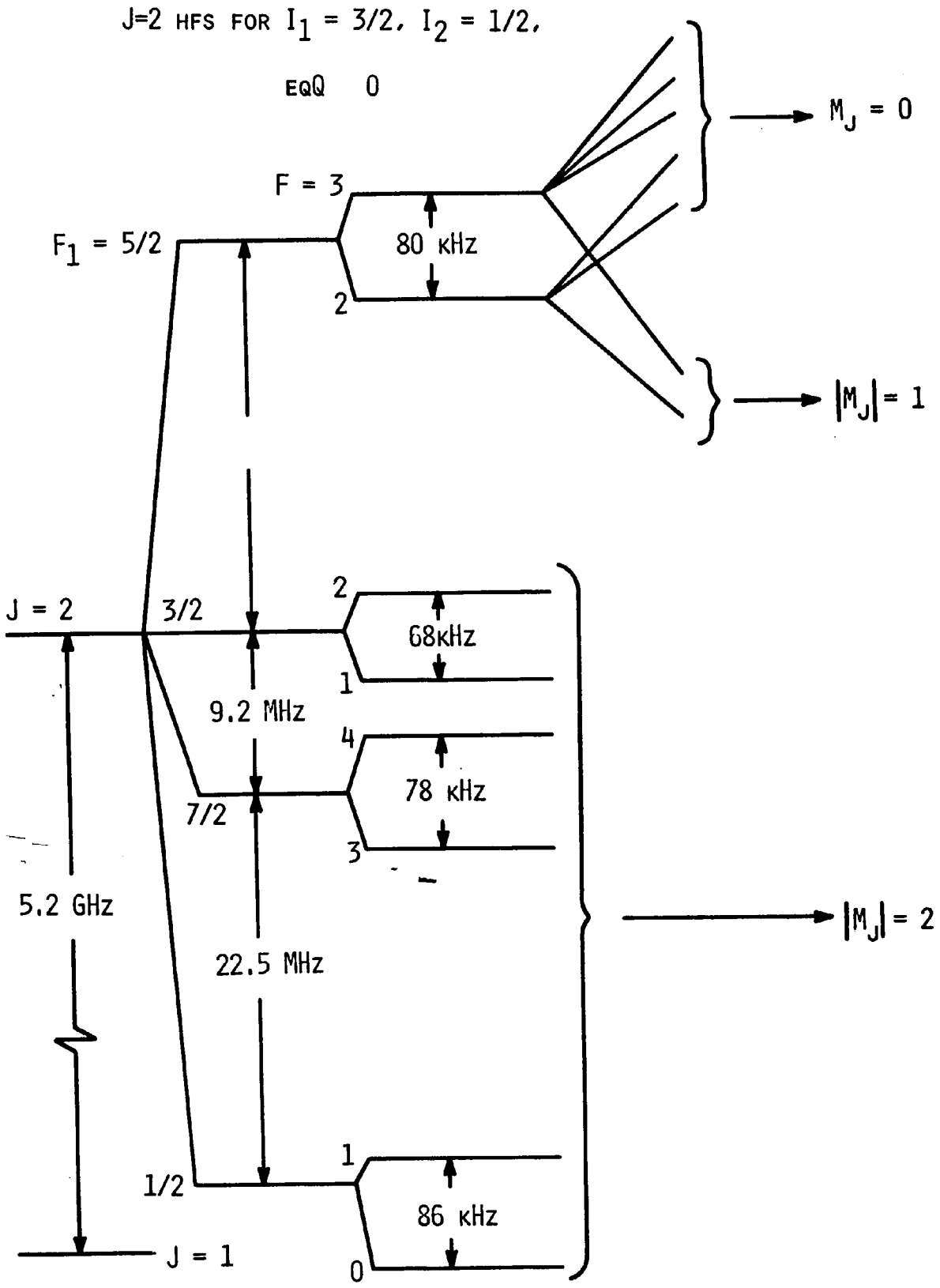


Figure IV(2) J = 2 Energy Level Diagram of TlBr.

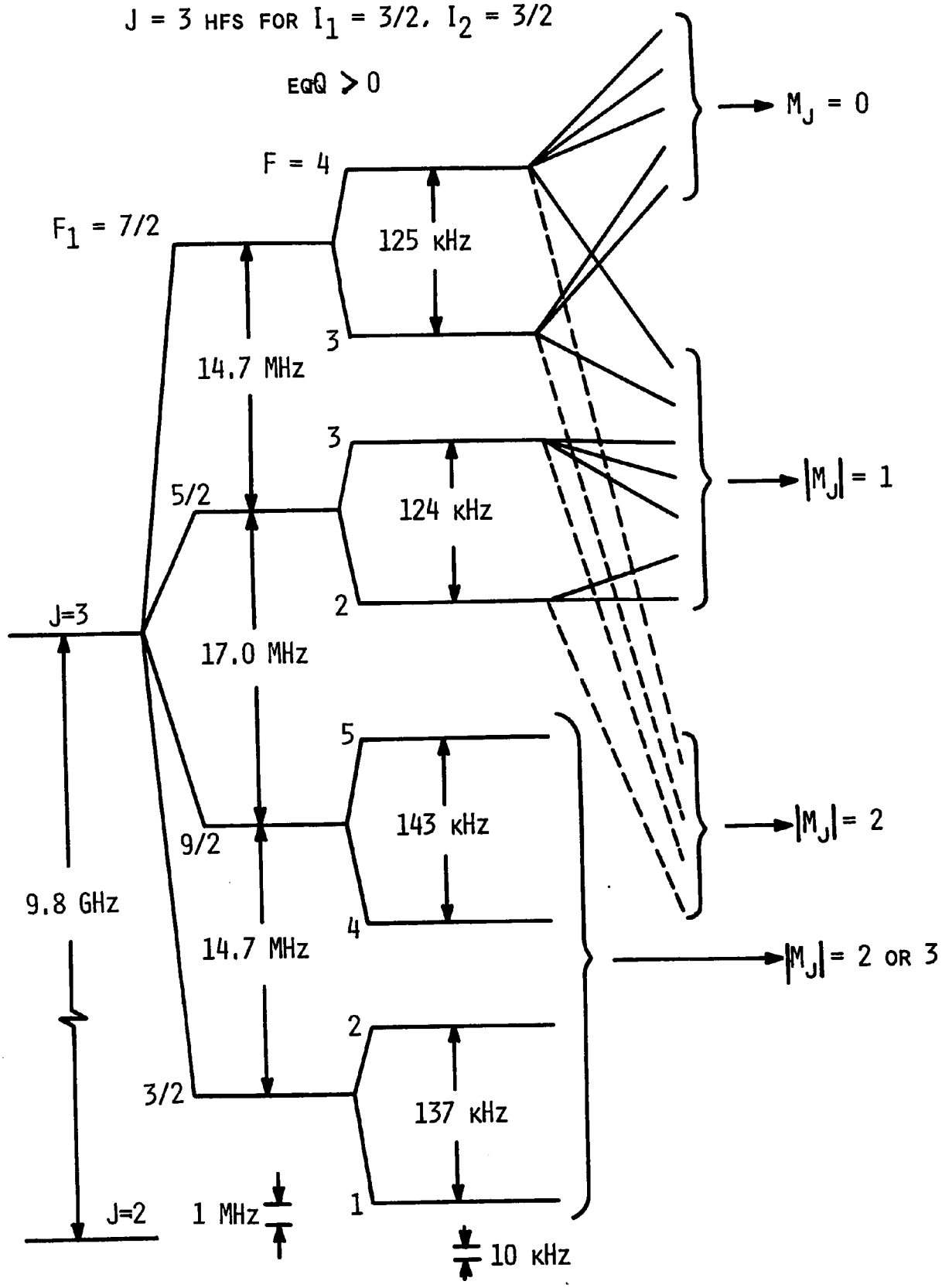


Figure IV(3) J = 3 Energy Level Diagram for TlBr.

$F_1 = 7/2$ level. As shown in Appendix C, the intensities of the $J = 3$ transitions are expected to be greater than those of $J = 2$ on the basis of the effective aperture of the focusing fields of the two J, $M_J = 0$ states. However, experimentally the $J = 3$ lines were observed to be smaller, in most cases, than the $J = 2$ lines. In fact, several of the $J = 3$ allowed transitions out of the $F_1 = 7/2$ level were too weak to measure. From the rather large size of some of the observed $J = 3$ transitions, it appeared that the populations of the two focused levels of $F_1 = 7/2$ were quite substantial. Hence the reduced intensity of the other $J = 3$ lines was believed to be due to smaller transition probabilities.

IV.D. Computer Treatment of Data

The hyperfine interaction constants of the molecule are calculated from the measured transition frequencies by means of a computer program written for the IBM 360/67 Michigan Terminal System. The program is written in double precision to avoid round-off errors in the calculations. The program first treats each energy level as being a linear combination of the hyperfine constants

$$E_{J,F_1F} = \sum_{i=0}^{4} c_i \cdot G_{J,F_1,F} \qquad \text{IV(2)}$$

where the ith coefficient, $G^i_{J,F_1,F}$ represents the diagonal matrix element of the ith hyperfine interaction operator (calculated according to the formulas in Table II(1)). The transition frequencies are then written as differences in

the hyperfine energies:

$$f_{(F_1,F) \rightarrow (F_1',F')} = \sum_{i=0}^{4} c_i \cdot g^i(J)_{(F_1,F) \quad (F_1',F')} \qquad IV(3)$$

where $g^i(J)_{(F_1,F)\rightarrow(F_1',F')} = G^i_{J,F_1,F} - G^i_{J,F_1',F'}$. A weighted-least squares subroutine then calculates the c_i's from the set of linear equations, where the frequencies may be weighted arbitrarily. The least squares method takes advantage of the fact that usually there are more measured transition frequencies than there are interaction constants to be determined. Consequently, the constants are usually over-determined. The least-squares method provides the "best" set of constants to fit the observed data.

The effect of the off-diagonal matrix elements on the energy levels, and therefore on the frequencies, can be included by means of corrections to the input frequencies. The off-diagonal matrix elements considered in our calculations are those involving:

1. The bromine quadrupole interaction ($J' = J \pm 2$)

2. The magnetic interactions of the thallium nucleus, i.e., those involving c_2, c_3, and c_4 ($F_1' = F_1 \pm 1$).

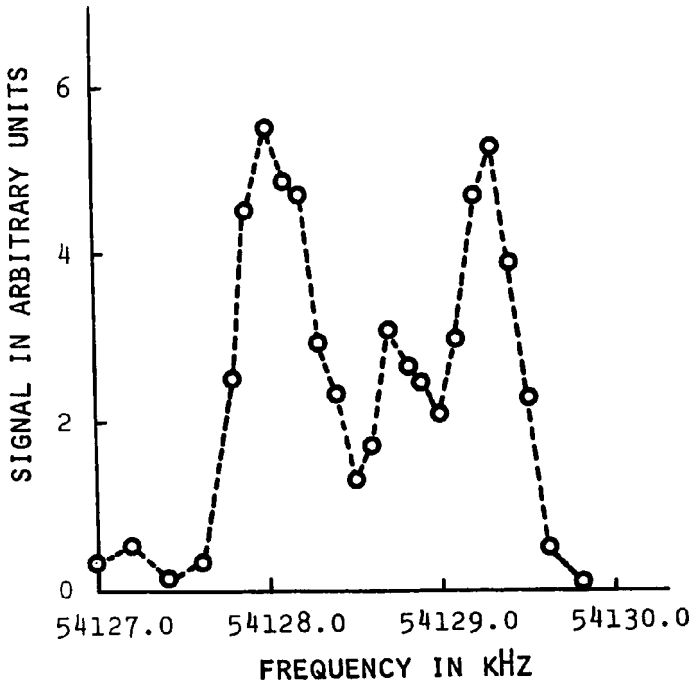
The corrections to the input frequencies may be written as algebraic expressions of the off-diagonal matrix elements, and therefore depend on the interaction constants. For example, the corrections due to (1) are found from Eq. II(5), and depend on eqQ and B_v. An iterative process is used in which the frequency corrections are computed using eqQ, c_2, c_3, and c_4 from the previous iteration. The corrected

frequencies are then least squared, resulting in new hyperfine interaction constants. This process is repeated until the constants do not change significantly from one iteration to the next. In the TlBr calculations, four or five iterations were sufficient for convergence of the constants to within very small limits.

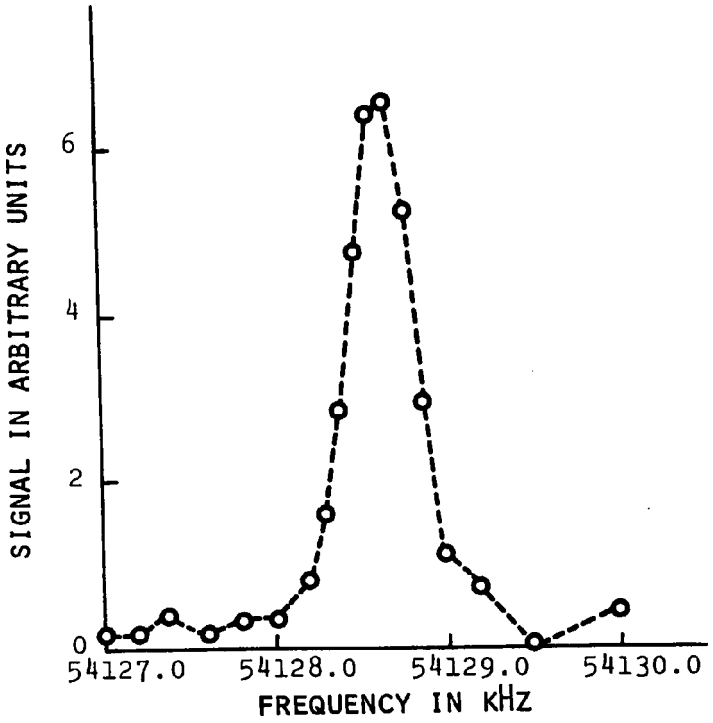
IV.E. Sources and Estimates of Errors

As mentioned previously, the transitions are measured in the presence of very weak electric and magnetic fields. The Zeeman effect in the earth's magnetic field can change the line shape and position significantly. This is illustrated in Figure IV(4a) for a J = 2, v = 0 line. The field conditions for this observation were E_{dc} = 1.5 v/cm, E_{rf} = 1.5 v rms/cm, and H = earth's magnetic field (approximately 0.6 gauss). In Figure IV(4b) the same transition is shown with H less than 50 milligauss. Tests for Zeeman shifts and splittings have been made at slightly higher magnetic fields (100 milligauss) on a few J = 2 transitions with no measurable effect on the lines observed. The Zeeman effect can be ignored in the analysis of the data since all final spectral lines were taken at magnetic fields below 50 milligauss.

The influence of the electric field on the observed transitions was investigated at various values of E_{dc} and E_{rf}. For example, all of the J = 2, v = 0 lines for $Tl^{79}Br$ were observed at E_{dc} = 1.0 v/cm, as well as E_{dc} = 1.5 v/cm.



(a) β_3 Tansition Observed with H = Earth's Magnetic Field (~0.6 gauss).



(b) β_3 Transition Observed with H < 50 milligauss.

Figure IV(4) Influence of Earth's Magnetic Field on the J = 2, v = 0 (5/2,3) → (1/2,1) Transition (α_2) in $Tl^{79}Br$.

The lines became narrower (i.e., the resolved lines narrowed from 500 Hz to 450 Hz) and better resolved as the E field was reduced. Shifts in line centers with this reduction in E_{dc} were typically 50Hz. The high frequency Stark effect [Marple and Trischka, (1956); Schlier (1957)] did not affect the observed transitions noticeably as long as the applied rf voltage was kept below 2.5 v rms. (At the rf and dc voltages used in this experiment, the static Stark effect is estimated to contribute approximately two times more than the high frequency Stark effect to the frequency shifts.) Figure IV(5) illustrates the effect of changing both the dc and rf voltages on a J = 2 transition.

The majority of the lines were measured at $E_{rf} \cong 1.3$ v rms/cm and $E_{dc} = 1.5$ v/cm; in weaker fields the reduction in signal made the measurements too difficult, and in some cases impossible. Thus, the small Stark shifts present at these fields were accepted as unaviodable errors. We estimate that in TlBr these errors are less than 100 Hz.

The only other major source of error in this experiment is in the choice of line centers previously discussed in Sec. IV.C.

The above errors are not random, so their effect on the calculated constants is not easy to assess. An estimate of the errors in the constants has been made on the basis of the scatter of the constants as different weights are assigned to the input frequencies. If one examines the resulting constants for different sets of weights, the constants are seen to be consistent to within particular limits, which

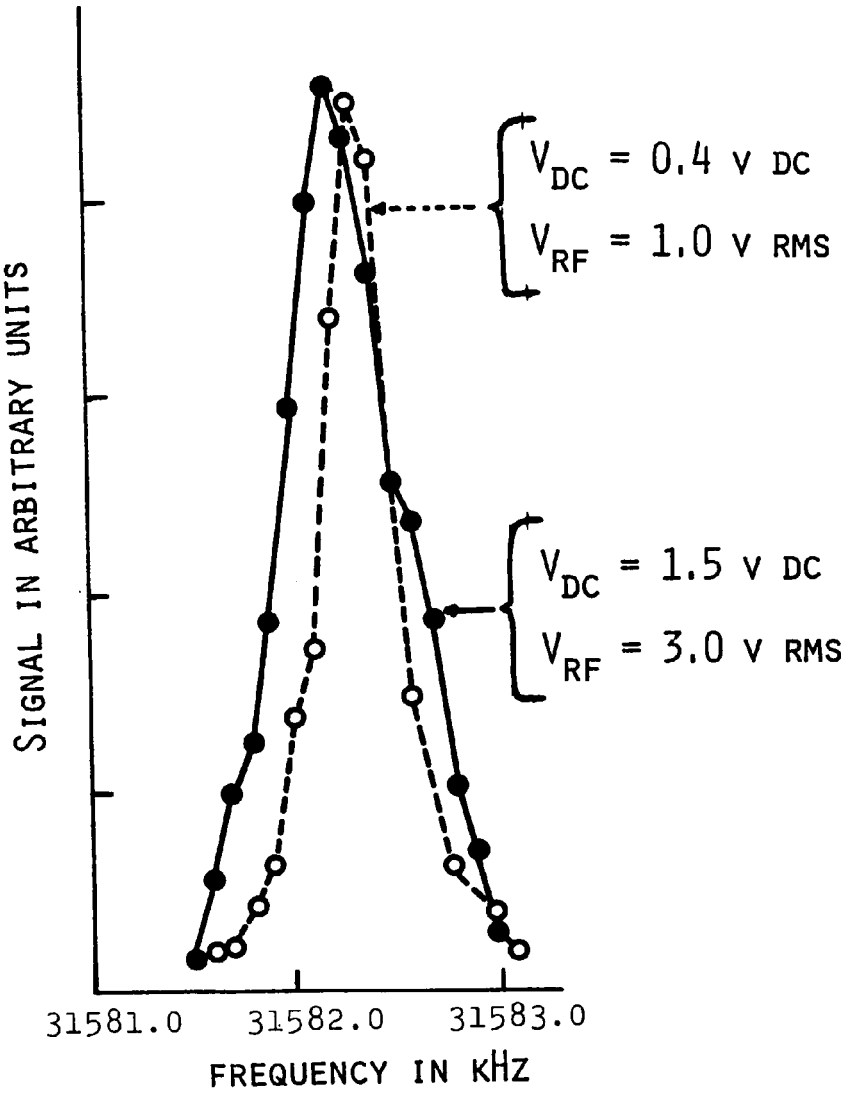


Figure IV(5) Effect of Changing V_{dc} and V_{rf} on the $J = 2$, $v = 0$ $(5/2,3) \rightarrow (7/2,4)$ Transition (β_3) in $Tl^{79}Br$.

are indications of the precision of the constants. These limits are used as guides to assign errors to the calculated constants.

IV.F. Calculated Constants

Table IV(3) lists the calculated hyperfine interaction constants for the J = 2 spectra observed. For most of the isotopes and vibrational states there was a sufficient number of measured lines to determine all five interaction constants with considerable confidence.

For some of the data sets in the higher vibrational states, however, there were too few lines to determine all of the constants. In these cases, reasonable values for some of the constants, say c_3 and c_4, could be provided from their expected behavior with vibrational state, and the remaining constants calculated from the measured lines. (The constants predicted from their behavior with v are marked by a * in Table IV(3).)

All of the v = 4 constants quoted in Table IV(3) are predicted values. (marked by †)

The hyperfine interaction constants obtained for J = 3, v = 0 are shown in Table IV(4). These constants are presented under the headings $Tl^{79}Br$ and $Tl^{81}Br$ because the lines corresponding to the two thallium isotopes were not resolvable at all. Because there were not enough lines to determine all of the constants for $Tl^{81}Br$, values of c_3 and c_4 (marked by ‡) were taken equal to those of J = 2, v = 0, $^{205}Tl^{81}Br$.

This was a reasonable step because c_3 and c_4 were found not to change appreciably with J in $Tl^{79}Br$.

Table IV(3)

J=2 Hyperfine Interaction Constants for TlBr

v=0

Tl Br	eqQ	c_1	c_2	c_3	c_4
205,79	126310.88(10)	3.690(5)	42.74(5)	-1.65(5)	-6.35(5)
205,81	105516.34(20)	3.915(5)	42.02(5)	-1.77(5)	-6.84(5)
203,79	126310.96(20)	3.691(10)	42.55(8)	-1.55(8)	-6.39(8)
203,81	105516.50(20)	3.909(10)	41.83(8)	-1.68(8)	-6.91(8)

v=1

205,79	126808.31(20)	3.681(8)	42.60(5)	-1.67(5)	-6.28(5)
205,81	105928.26(20)	3.908(8)	41.85(5)	-1.79(5)	-6.81(5)
203,79	126808.75(25)	3.687(10)	42.14(8)	-1.68(8)	-5.95(8)
203,81	105928.73(25)	3.915(10)	41.59(8)	-1.73(8)	-6.76(8)

v=2

205,79	127302.61(20)	3.67(2)	42.43(8)	-1.68(8)	-6.28(8)
205,81	106337.52(20)	3.89(2)	41.72(8)	-1.78(8)	-6.77(8)
203,79	127303.64(25)	3.68(2)	42.15(10)	-1.68(8)	-6.15(10)
203,81	106338.39(25)	3.94(2)	41.44(10)	-1.71(8)	-6.52(10)

v=3

205,79	127793.58(30)	3.66(3)	42.31(10)	-1.66*	-6.12*
205,81	106746.05(30)	3.88(3)	41.62(10)	-1.79(10)	-6.79(10)
203,79	127795.20(30)	3.68(3)	42.00(10)	-1.68*	-6.12*
203,81	106744.19(30)	3.89(3)	41.52(10)	-1.86(10)	-6.90(10)

Table IV(3) (Continued)

		v=4			
205,79	128281.82†	3.65†	42.22†	-1.66†	-6.04†
205,81	107148.06†	3.870†	41.52†	-1.78†	-6.73†

*Values predicted from change in c_3 and c_4 with v.

†Values predicted from change in constants with v.

Table IV(4)

J=3, v=0 Hyperfine Interaction Constants for TlBr

$Tl^{79}Br$	126311.26(25)	3.700(10)	42.80(25)	-1.66(8)	-6.33(8)
$Tl^{81}Br$	105516.78(30)	3.918(10)	41.90(30)	-1.77†	-6.84†

†Values taken from J=2, v=0.

CHAPTER V

INTERPRETATION OF RESULTS

V.A. Verification of Hamiltonian

When many spectral lines are used to determine a few interaction constants, good agreement between the theory and calculations implies that the Hamiltonian is complete and the line assignment is correct. In the TlBr spectra analyzed in this experiment the fit of the transition frequencies calculated from the interaction constants onto the observed spectrum was extremely good. (All predictions fell within ± 100 Hz of the line centers.) The average fit of a particular spectrum was generally found to reflect the level of confidence in the line centers determined for that spectrum. For example, the average fit of the $J = 2$, $v = 0$ ^{205}TlBr spectra was 30 Hz, while the average fit of the $J = 2$, $v = 2$ ^{203}TlBr spectra was 50 Hz.

In preliminary analysis of the data, the bromine octupole interaction was added to the Hamiltonian of Eq. II(11) and used in the calculation of the constants. Although there was a very slight improvement of the fit, the octupole contributions to the line frequencies were quite small (50 Hz) with very small changes in the other five constants. As a consequence, there was no basis for

considering a non-zero magnetic octupole interaction in the final analysis of the data.*

V.B. The Quadrupole Interaction

From our measurements we were able to determine the bromine quadrupole interaction constant (eqQ) for the various isotopes and v and J states to a precision of a few parts in 10^6. In the interpretation of these results we are not always able to make full use of this precision since the existing theories of the quadrupole interaction for molecules containing heavy atoms are very approximate. However, it is felt worthwhile to consider a few topics concerning the interpretation of the measured values of eqQ in TlBr.

V.B.1. The Ionic Character of the Thallium-halides

The most successful theoretical description of the quadrupole interaction at the halogen nucleus of an alkali-halide molecule is that of the deWijn model (1966). deWijn gives the following expression for the field gradient at the halogen nucleus:

$$q_{Halogen} = i\frac{\alpha_2 e^2}{6W R_e^4} q_{n10} \left[1 + \frac{2\alpha_1}{R_e^3}\right]^2 + (1-i)(-q_{n10}) \qquad V(1)$$

where: i = ionic character of the molecule

α_2 = the polarizibility of the free halogen ion

e = charge of the electron

---

*The nuclear hexadecapole interaction cannot exist in TlBr because both I_1 and I_2 are less than 2. For a discussion of our search for this effect in TlI (the spin of iodine is 5/2) see Stephenson (1968).

W = ionization potential of the halogen atom

R_e = equilibrium internuclear separation

q_{n10} = the electric field gradient at the nucleus of the halogen atom due to the valance electron in a np orbital with m = 0.

α_1 = the polarizibility of the free metal ion.

This expression has been used by deWijn to determine i, the ionic character (Pauling, 1960, p. 94), for several of the alkali-halides, where $q_{halogen}$ is computed from experimental values of eqQ for these alkali-halides and known quadrupole moments. In Table V(1) we list deWijn's results for the lithium-halides.

Table V(1)

Ionic Character of Lithium-Halides*

Molecule	$q_{Halogen}$ ($\times 10^{15}$ esu)	i (ionic character)
LiCl	+ .53	0.85
LiBr	+1.5	0.83
LiI	+3.5	0.78

*These quantities are taken from Table IV of (deWijn, 1966).

Using Eq. V(1), we may calculate the ionic character for the thallium-halides, where the $q_{halogen}$ are determined from our measured values of eqQ (and known quadrupole moments). Table V(2) lists these values.

Table V(2)

Ionic Character of Thallium-Halides

Molecule	$q_{Halogen}$ ($x10^{+15}$ esu)	i (ionic character)
TlCl	2.75	0.77
TlBr	5.60	0.71
TlI	7.65	0.68

(The necessary values of α_1, α_2, W, q_{n10} were taken from the same references used by deWijn; the values of R_e are due to Fitzky.)

The values of i obtained for the thallium-halides are seen to be slightly smaller than those for the lithium halides, indicating that the bond is less ionic in the case of the thallium-halides. This decrease in i agrees with the expected change due to the decrease in electronegativity from lithium to thallium (Pauling, 1960, p. 94).

In both the lithium- and the thallium-halides, the ionic character is seen to decrease from chlorine to iodine, which again is in accordance with electronegativity differences.

It is of interest to note that the relatively large values of $q_{halogen}$ in TlBr and TlI, in terms of the deWijn model, are primarily due to the relatively low ionic character of these molecules; a lower ionic character results in a decrease of the quenching of the polarization of the halogen electron orbitals that are directed along the internuclear axis.

V.B.2. The Dependence of eqQ on v

The change of eqQ with vibrational state is about a 0.4% effect and leads to shifts in frequency of several tens of kHz. The dependence of eqQ on v, the vibrational state, is conveniently expressed in the power series:

$$eqQ_v = \underline{a} + \underline{b}\ (v+\tfrac{1}{2}) + \underline{c}\ (v+\tfrac{1}{2})^2 + \ldots \qquad V(2)$$

where eqQ_v is the quadrupole interaction constant of the vth vibrational state, and $\underline{a}$, $\underline{b}$, and $\underline{c}$ are the coefficients of the expansion. For most molecules studied with present-day precision, the first three terms of this expansion are adequate for describing the observed behavior of eqQ_v as a function of v. The values of $\underline{a}$, $\underline{b}$, and $\underline{c}$ for J = 2 and all four isotopic species are given in Table V(3).

Table V(3).

Constants Related to Dependence of eqQ on v*

Expansion Coefficients for Eq. V(2)	$^{205}Tl^{79}Br$	$^{203}Tl^{79}Br$	$^{205}Tl^{81}Br$	$^{203}Tl^{81}Br$
$\underline{a}$	126060.99	126060.97	105309.38	105309.42
$\underline{b}$	500.56	500.69	414.58	414.80
$\underline{c}$	-1.57	-1.45	-1.33	-1.28
for Eq. V(3)				
A	126062	126062		
B	247425	249153		
C	258497	259202		

*All constants are given in kHz.

The changes in eqQ with v are related to the fact that q, the electric field gradient at the halogen nucleus, is a function of the internuclear separation, R. However, the expectation values of various powers of R, $\langle v|R_n|v\rangle = \langle R^n\rangle_v$, are dependent on v because V(R), the internuclear potential, is anharmonic.

The dependence of eqQ on R^n can be expressed by the following expansion:

$$eqQ_v = A + B\langle\rho\rangle_v + C\langle\rho^2\rangle_v + \cdots \qquad V(3)$$

where $\rho = \dfrac{R-R_e}{R_e}$.

The expectation values of the various powers of ρ may be related to the values of $\langle(R/R_e)^2\rangle$ known from the measured B values of the molecule (Fitzky, 1958), where use is made of the relations given by Ramsey (1956, p. 231) between $\langle(R/R_e)^n\rangle_v$ and other molecular constants (ω_e, B_e, and α_e). We have carried out the determination of the expansion coefficients of Eq. V(2) for the J = 2 values of eqQ in $^{205}Tl^{79}Br$ and $^{203}Tl^{79}Br$. These are listed in Table V(3).

Zeiger and Bolef (1952) have derived the following relationships between the coefficients of the two expansions given by Eq. V(2) and V(3):

$$\underline{a} = \underline{A} \qquad V(4)$$

$$\underline{b} = B_e/\omega_e \; 3(1 + \alpha_e\omega_e/6B_e^2)\; \underline{B} + 2\underline{C} \qquad V(5)$$

First, from the values listed in Table V(3) we note that $\underline{a}$ and $\underline{A}$ are indeed nearly equal. This justifies the statement

that the more precisely determined $\underline{a}$ represents the value of eqQ when the internuclear separation, R, is equal to the equilibrium value, R_e. This will be of use to us later.

Second, we can compare our measured values of $\underline{b}$ (500.56 kHz and 500.67 kHz for $^{205}Tl^{79}Br$ and $^{203}Tl^{79}Br$, respectively) with the values obtained from Eq. V(5): $\underline{b}^{205}$ = 490 kHz and $\underline{b}^{203}$ = 493 kHz.

The deWijn model also yields a prediction for the first order change in eqQ with vibrational state due to the change in $\langle R^n \rangle_v$ with v. His expression for $\underline{b}$ is:*

$$\underline{b} = eQ \frac{B_e}{\omega_e} \left[(20 + 12a_1) + 4 \frac{\alpha_1}{R_e^3} (56 + 21a_1) \right] \frac{\alpha_2 e^2}{6W R_e^4} q_{n10} \qquad V(6)$$

where a_1, a constant related to the first anharmonic term in the internuclear potential, may be written in terms of other molecular constants as follows:

$$a_1 = -(1 + \frac{\alpha_e \omega_e}{6 B_e^2}). \qquad V(7)$$

If we evaluate Eq. V. (6) for $^{205}Tl^{79}Br$ we obtain a predicted value of 730 kHz, which is only in modest agreement with the experimentally observed value of 500 kHz [Table V(3)]. Similar agreement is seen in the other isotopic species.

Another interesting effect related to the change in eqQ with v is shown when we consider the difference in corresponding quadrupole interaction constants for the two thallium isotopes, i.e.,

---

*deWijn's expression is actually $q(v) = \underline{b}/eQ$.

$$\Delta = eqQ_{^{203}Tl^{79}Br} - eqQ_{^{205}Tl^{79}Br}, \qquad V(8)$$

as a function of v. Δ vs. v is plotted in Figure V(1) [the larger dots]. We note that although for v = 0 the corresponding values of eqQ are very nearly equal, they differ significantly as v increases. Since eqQ as a function of v for each isotopic species is well described by Eq.V(2), we may form the function Δ. For the $Tl^{79}Br$ isotopes we find:

$$\Delta_{79}(Hz) = 93 + 245v + 115v^2 \qquad V(9)$$

This expression is plotted in Figure V(1) as the solid line. It is clear that for higher v, the term in v^2 contributes significantly to Δ.

We thus have a very sensitive effect due to the small change in mass from $^{203}Tl^{79}Br$ to $^{205}Tl^{79}Br$. Unfortunately the theories of the quadrupole interaction are not able to verify this effect quantitatively. From Zeiger and Bolef's equation [Eq. V(5)] we predict a $\Delta(Hz) \doteq 3000\,v$, which is obviously too large, but at least of the correct sign. The deWijn model predicts a $\Delta(Hz) = -3200$ v, wrong in both sign and magnitude.

Exactly the same effect occurs in the $Tl^{81}Br$ species. The experimentally determined Δ_{81} is fit quite well by the solid curve in Figure V(1).

V.B.3. The Dependence of eqQ on J

Zeiger and Bolef also give an expression for the dependence of eqQ on J, from which the change in eqQ when J is

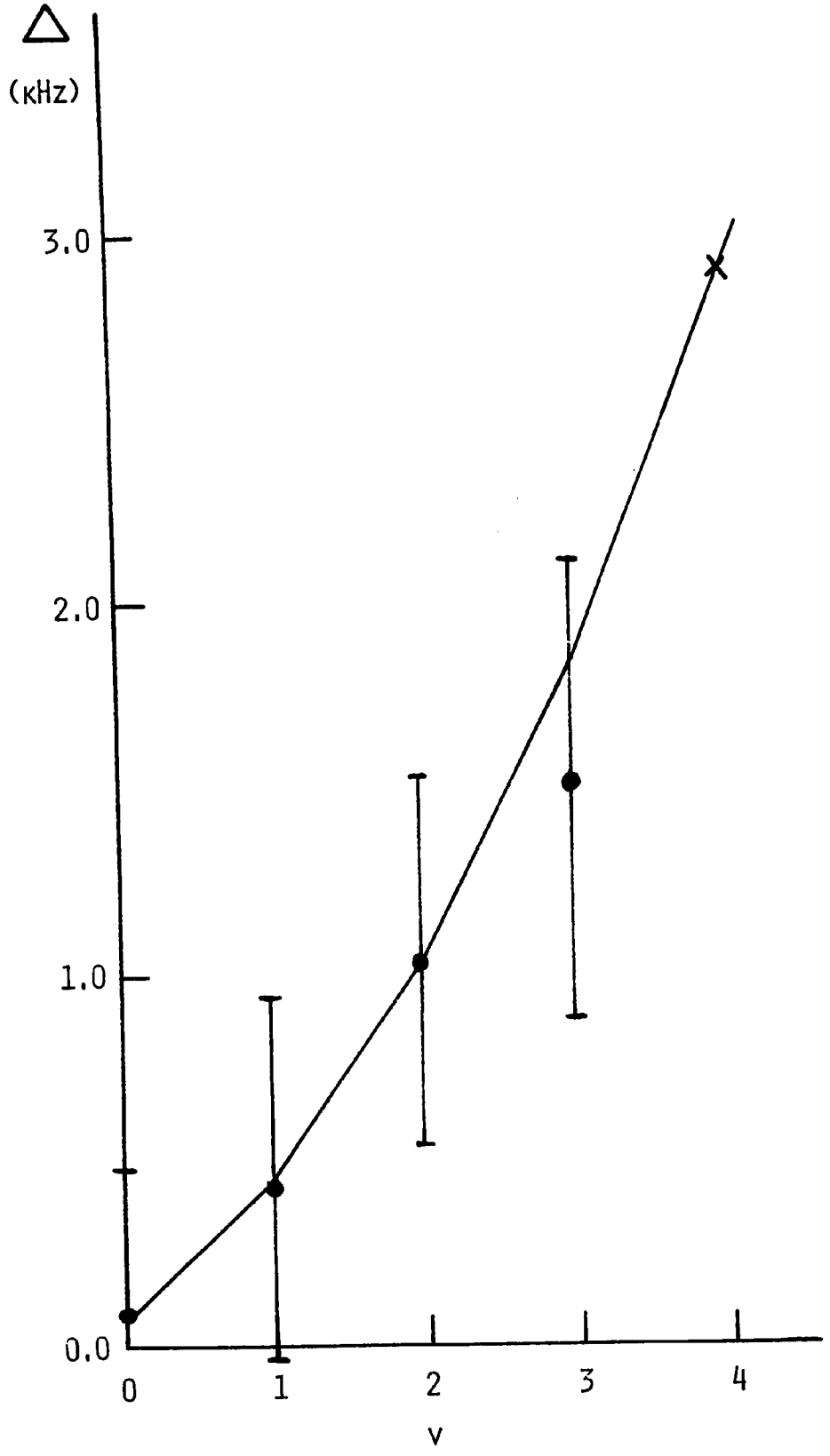


Figure V(1) The Quantity $\Delta = eqQ_{^{203}Tl^{79}Br} - eqQ_{^{205}Tl^{79}Br}$ plotted as a function of v.

increased by one can be

$$\Delta eqQ_{J \rightarrow J+1} = (2J + 1)\left(\frac{2B_e}{\omega_e}\right)^2 \underline{B} \qquad V(10)$$

when $\underline{B}$ is the second coefficient of Eq.V(3). For the change of J from J = 2 to J = 3 the predicted change is +50 Hz. Experimentally the observed changes are:

$+ 380 \pm 300$ Hz in $Tl^{79}Br$

$+ 440 \pm 400$ Hz in $Tl^{81}Br$.

V.B.4. False Quadrupole Effects

There are other effects which contribute to the variation of energy with nuclear orientation in much the same way as the nuclear quadrupole interaction. These include the so-called "pseudo-quadrupole effect" and the polarization of the nucleus by electric fields.

The pseudo-quadrupole effect is the result of a second order magnetic interaction between the electron orbital angular momentum and the nuclear magnetic moment. The interaction has the form:

$$W_{PSQ} = \frac{\langle o|a\vec{I}_1 \cdot \vec{L}|n\rangle^2}{W_n - W_o} \qquad V(11)$$

where:

$\vec{L}$ is the total electronic orbital angular momentum

$|n\rangle$ is the electronic wave function of the nth excited state

W_n, W_o are the energies of the excited and ground electronic states, respectively

and:

$$a = \frac{2\mu_I \mu_{ON}}{I} \langle 1/r^3 \rangle_{Av} \qquad V(12)$$

where:

μ_I is the nuclear magnetic moment

μ_{ON} is the nuclear magneton

$\vec{I}_1$ is the nuclear spin angular momentum

r is the average distance from nucleus 1 to the valance electron

$\langle 1/r^3 \rangle_{AV}$ is the average over the excited electronic states of $1/r^3$.

In a ^{1} diatomic molecule $\vec{L}$ may be thought of as precessing about the molecular axis with a projection of zero onto this axis. Therefore, $\vec{I} \cdot \vec{L}$ is proportional to the cosine of the angle between $\vec{I}$ and the molecular axis, and the energy, W_{PSQ}, is then proportional to the square of this cosine. This is identical to the behavior of the quadrupole interaction, and it is therefore impossible to distinguish between the two effects with the information from one molecular species alone.

We may estimate the size of W_{PSQ} in the following way. First, the Eq.V(9) for W_{PSQ} is written:

$$W_{PSQ} = \left[\frac{2\mu_I \mu_{ON}}{I} \langle 1/r^3 \rangle_{AV} \right]^2 \sum_n \frac{\langle o|L_i|n\rangle^2}{W_n - W_o} \qquad V(13)$$

where L_i is the component of L along the nuclear spin axis. White (1955) suggests an approximation for $\langle 1/r^3 \rangle_{AV}$, namely $\frac{1}{2}(1/r^3)^{ATOM}_{AV}$ which is $\frac{1}{2}$ of the average value of $1/r^3$ for the valance electron in the first excited p-orbital of the neutral atom. The factor $\frac{1}{2}$ is an estimate of the necessary correction

to the value of $(1/r^3)_{AV}^{ATOM}$ for placing the atom into a two atom molecule. White also shows how the quantity

$$\sum_n \frac{|\langle o|L_i|n\rangle|^2}{W_n - W_o}$$

can be evaluated from the spin-rotation interaction constant of the nucleus in question. For the bromine nucleus in TlBr one finds:

$$\langle 1/r^3\rangle_{AV} = 4.6 \times 10^{25} \text{ cm}^{-3}$$

$$\frac{|\langle o|L_i|n\rangle|^2}{W_n - W_o} = 1.7 \times 10^{-42} \text{ gm cm}^2$$

so that with the known values of μ_I and I for the bromine nucleus one obtains W_{PSQ} which for $I_1 = 3/2$ yields $eqQ_{PSQ} = 2.4$ kHz. With typical uncertainties of ± 300 Hz on the measured values of eqQ we see that the pseudoquadrupole effect may certainly be significant if we wish to evaluate the true quadrupole interaction.

A second "false quadrupole effect" may be due to nuclear polarization (Townes, 1958, p. 402). The strong electrostatic field at the nucleus 1 due to the electrons and other nucleus induces a small electric dipole moment in the nuclear charge distribution which tends to increase the attractive force between the electron and nucleus, thereby lowering the electronic energy levels by an amount which depends on the nuclear polarizability and the square of the electric field strength. Since the nuclear polarizability along the spin axis is not necessarily the same as the polarizability

perpendicular to this axis, the energy depends on the orientation of the spin with respect to the electric field. Gunther-Mohr, Geschwind, and Townes (1951) have shown this energy to vary with orientation just like the quadrupole interaction. Its contribution to the measured quadrupole interaction may be shown to be:

$$eqQ_{NP} = 2/3\ (\alpha_z - \alpha_x)\ ep \qquad V(14)$$

where α_z and α_x are the components of the nuclear polarizability parallel and perpendicular to the spin axis

e = electron charge

$$p = \left\langle \frac{\rho 3(\cos^2\theta_m - 1)}{r^4} \right\rangle_{av}$$

and ρ = charge density outside the nucleus considered

θ_m = angle between symmetry axis of molecule and charge

r = distance from nuclear center to charge.

A rough estimate of $\alpha_z - \alpha_x = \Delta\alpha$ may be obtained by setting it equal to the nuclear volume, so that $\Delta\alpha = 10^{-38}$ cm^3. An estimate of p can be made from the known value of the field gradient, q_{Br}, and an estimate of $(1/r^4)_{Av}$, since $p = q\ (1/r^4)_{Av}/(1/r^3)_{Av}$.

Gunther-Mohr, et al. show that $\langle 1/r^4\rangle_{Av} = 7.5\ \langle 1/r^3\rangle_{Av}^{4/3}$ for a 3p electron, as in Cl. We shall assume that the two average values for Br are related in the same way.

This yields an estimate of eqQ_{NP}:

$$eqQ_{NP} = 2/3\ eq\ (\Delta\alpha)\ (7.5)\ (1/r^3)_{Av}^{1/3} \qquad V(15)$$

$$= 30 \text{ kHz}$$

This estimate is, of course, quite rough and it is presented here primarily as a motivation for looking for such an effect.

As indicated earlier, the pseudoquadrupole effect and the nuclear polarization depend on nuclear orientation in exactly the same way as the quadrupole interaction. Consequently the measured value of eqQ is really equal to eqQ_{TRUE} + eqQ_{FALSE}, where $eqQ_{FALSE} = eqQ_{PSQ} + eqQ_{NP}$.

Now it is likely that both terms of eqQ_{FALSE} depend strongly on the environment in which the nuclei reside, so a study of the ratio of values of eqQ for two isotopes of the nucleus containing the quadrupole moment, as measured in different environments, could be used to look for the existence of false quadrupole effects.

In comparing ratios of eqQ in molecules we must correct for differences in vibrational motion due to the mass differences. This can be done by taking the ratio of the $\underline{a}$ constants, [Eq. V(2)] which we have previously identified as the value of eqQ for $R = R_e$. To within the precision of microwave data, the equilibrium internuclear separations are the same for different isotopic species of diatomic molecules such as the alkali- and thallium-halides. It is therefore justifiable to assume that if $eqQ_{FALSE} = 0$, the values of $q_{79}(R_e)$ and $q_{81}(R_e)$ are equal, so that the ratio $\underline{a}_{79}/\underline{a}_{81}$ should be equal to Q_{79}/Q_{81}, the ratio of the nuclear quadrupole moments.

We have chosen to compare our measured values of eqQ

for $Tl^{79}Br$ and $Tl^{81}Br$ with the ratios of the quadrupole constants in free bromine atoms as determined by Brown and King (1966). The ratios are shown plotted in Figure V(2) showing the differences in the ratios between TlBr and the Br atoms to be quite small, about $4 \pm 4 \times 10^{-6}$. To make meaningful comparisons of these ratios to a few parts per million requires a very careful examination of our assumptions; in particular, does $q_{79}(R_e)$ equal $q_{81}(R_e)$ to within the necessary accuracy? This in itself is a very formidable problem. Hence, we present the results of this analysis as an open question as to whether the small observed difference in the ratios represents evidence of a false quadrupole effect. We do point out, however, that the observed difference of approximately 4 ± 4 parts in 10^6 between $\underline{a}_{79}/\underline{a}_{81}$ in TlBr and β_{79}/β_{81} is considerably less than the observed difference of about 2 parts in 10^5 between $\underline{a}_{79}/\underline{a}_{81}$ in LiBr (Hebert, 1964) and β_{79}/β_{81}.

V.C. Spin-Rotation Interactions

V.C.1. The Magnetic Fields at the Nuclei

As indicated in Chapter II, the spin-rotation interactions are due to the interaction of the nuclear magnetic moments with the magnetic fields produced by the molecule's rotation at the two nuclei. In TlBr, the spin-rotation interaction constants may be written:

$$C_{Br} = \frac{\mu_{Br} H_{Br}}{I_1} \quad \text{and} \quad C_{Tl} = \frac{\mu_{Tl} H_{Tl}}{I_2} \qquad V(16)$$

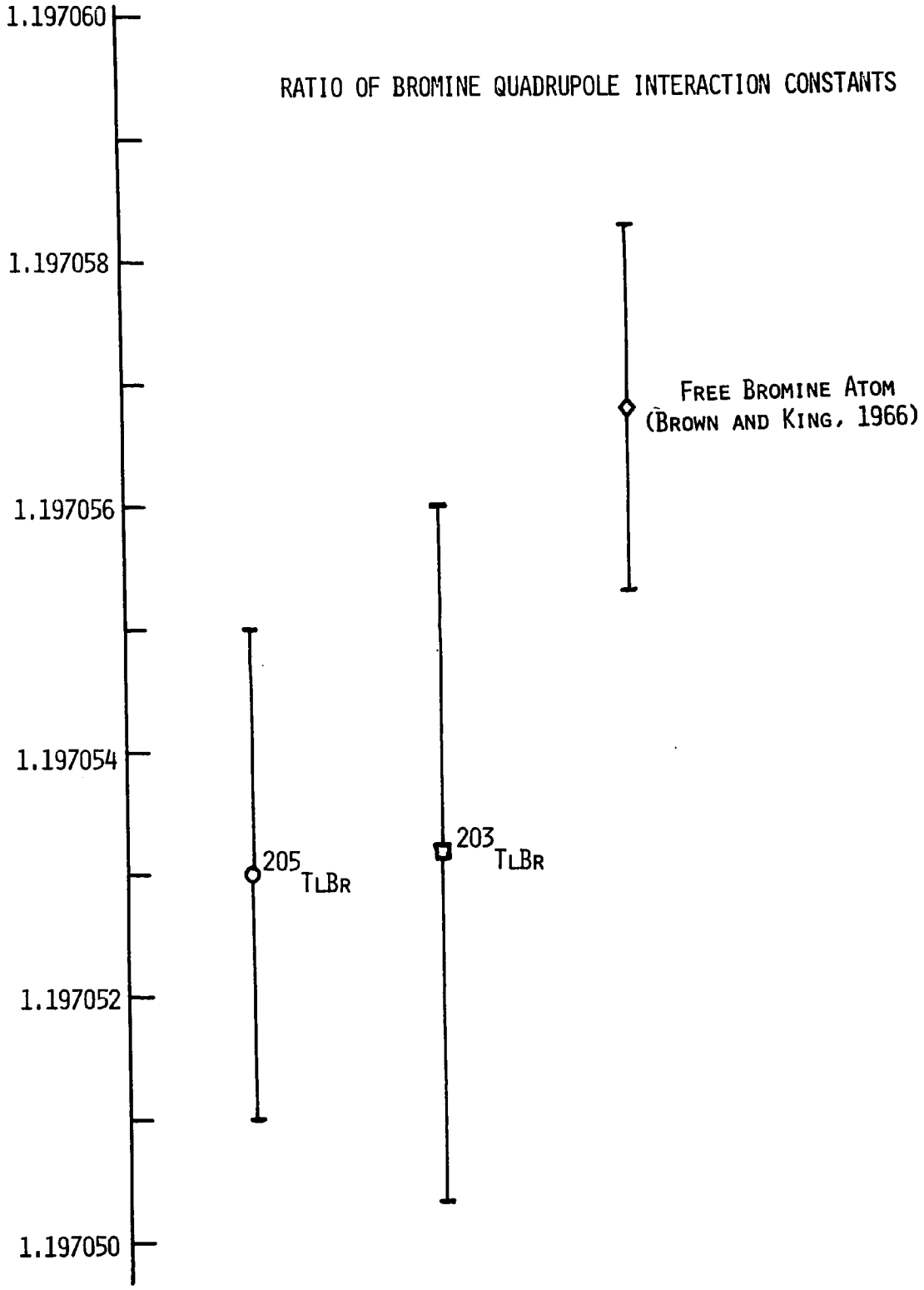


Figure V(2) Ratios of the Quadrupole Interaction Constants for ^{79}Br and ^{81}Br in TlBr and the Free Bromine Atom.

where H_{Br} and H_{Tl} are the magnetic fields at the nuclei. From the measured values of C_{Br} and C_{Tl} for $^{205}Tl^{79}Br$ in the $J = 2$, $v = 0$ states, we may calculate the magnetic fields at the two nuclei:

$$H_{Br} = 3.45 \text{ gauss} \quad H_{Tl} = 17.23 \text{ gauss.}$$

The fields are seen to differ to about a factor of five. The same effect, the much larger magnetic field at the thallium nucleus, occurs in the other thallium-halides.

The magnetic field, H_i, at the ith nucleus of a heavy diatomic molecule is almost entirely due to the small orbital angular momentum about the ith nucleus. White (1955) has shown that H_i is given approximately by:

$$H_i = 4\mu_{oB} B\langle 1/r_i^3\rangle_{Av} \sum_n \frac{|\langle o|L_x^i|n\rangle|^2}{W_n - W_o} \qquad V(17)$$

where μ_{oB} is the Bohr magneton, B is the rotational constant of the molecule, r_i is the distance of the valance electron from the ith nucleus, $\langle 1/r_i^3\rangle_{Av}$ is the average of $1/r_i^3$ over the excited electronic states, L_x^i is the component of total electronic angular momentum about the ith nucleus in the direction of $\vec{J}$, the rotational angular momentum of the molecule, $|n\rangle$ is the electronic wave function of the nth excited state, W_n is the energy of the nth excited electronic state. Evaluating $\langle 1/r_i^3\rangle_{Av}$ and $\langle o|L_x^i|n\rangle$ is difficult because we do not know the electronic wave functions. However, White has suggested an approximation for $\langle 1/r_i^3\rangle_{Av}$ which at least will allow us to compare $\langle o|L_x^i|n\rangle$ for the two nuclei in the molecule. From Eq. V(17) evaluated for both nuclei in the

same molecule, we obtain for the ratio of angular momenta:

$$\frac{\sum_n \frac{|\langle o|L_x^1|n\rangle|^2}{W_n - W_o}}{\sum_n \frac{|\langle o|L_x^2|n\rangle|^2}{W_n - W_o}} = \frac{H_1\langle 1/r_2^3\rangle_{Av}}{H_2\langle 1/r_1^3\rangle_{Av}} \qquad V(18)$$

White's approximation for $\langle 1/r^3\rangle_{Av}$ is to set it equal to $\frac{1}{2}\langle 1/r^3\rangle_{Av}^{Atom}$ (as we did in estimating the pseudoquadrupole effect), where values of $\langle 1/r^3\rangle_{Av}^{Atom}$ have been tabulated by Barnes and Smith (1954). H_1 and H_2 can be calculated from the measured c_1 and c_2 using Eq. V(16). We have evaluated Eq.V(18) for all the thallium-halides with the results:

TlF: Tl/F = 6.3

TlCl: Tl/Cl = 5.8

TlBr: Tl/Br = 5.7

TlI: Tl/I = 6.0

All the ratios are seen to be nearly the same, as one would expect from the similarity of the electronic structure of the Tl-halides. The implication of the above ratios is that the relatively large differences between H_{Tl} and $H_{halogen}$ are due to the substantial differences of the electronic angular momenta about the two nuclei in the molecule.

V.C.2. The Dependence of c_1 and c_2 on Isotope

Another interesting feature of the spin-rotation interactions are their dependence on the nuclear g-factors, g_i,

and the rotational constant of the molecule, B, namely, c_i is proportional to $g_i B$. If we compare the spin-rotation interaction constants for the same nucleus, i, but for different isotope we expect that, because of the similarity of electronic structure, the factor involving L_x^i and $1/r_i^3$ will remain unchanged. Hence the ratios of c_i's for different isotopes should be equal to the ratios of the corresponding $g_i B$, g_i, in nuclear magnetons, for the bromine and thallium isotopes are

$$g_{^{79}Br} = 1.3993 \qquad g_{^{81}Br} = 1.5084$$

$$g_{^{203}Tl} = 3.2230 \qquad g_{^{205}Tl} = 3.2480$$

For example, let us compare c_1 and c_2 obtained from the TlBr, $J = 2$, $v = 0$ spectra when we change bromine isotopes. [We make the following abbreviation: $^{205}Tl^{79}Br \equiv 205,79$.] The ratios of the spin-rotation constants are shown in the left hand column, and the appropriate ratio of $g_i B$ is shown opposite it in the right hand column.

$$c_1 \begin{cases} \dfrac{c_1\ _{205,79}}{c_1\ _{205,81}} = 0.943(5) & \dfrac{g_{79}}{g_{81}} \times \dfrac{B^{v=0}_{205,79}}{B^{v=0}_{205,81}} = 0.945 \\ \dfrac{c_1\ _{205,79}}{c_1\ _{203,81}} = 0.944 & \dfrac{g_{79}}{g_{81}} \dfrac{B^{v=0}_{203,79}}{B^{v=0}_{203,81}} = 0.944 \end{cases}$$

$$c_2\begin{cases} \dfrac{c_{2\ 205,79}}{c_{2\ 205,81}} = 1.017 & \dfrac{B^{v=0}_{205,79}}{B^{v=0}_{205,81}} = 1.018 \\ \hline \dfrac{c_{2\ 203,79}}{c_{2\ 203,81}} = 0.926 & \dfrac{B^{v=0}_{203,79}}{B^{v=0}_{203,81}} = 0.928 \end{cases}$$

Similarly we may change Tl isotope and again compare ratios:

$$c_1\begin{cases} \dfrac{c_{1\ 205,79}}{c_{1\ 203,79}} = 0.999 & \dfrac{B^{v=0}_{205,79}}{B_{203,79}} = 0.997 \\ \hline \dfrac{c_{1\ 205,81}}{c_{1\ 203,81}} = 1.001 & \dfrac{B^{v=0}_{205,81}}{B^{v=0}_{203,81}} = 0.997 \end{cases}$$

$$c_2\begin{cases} \dfrac{c_{2\ 205,79}}{c_{2\ 203,79}} = 1.005 & \dfrac{g_{205}}{g_{203}} \times \dfrac{B^{v=0}_{205,79}}{B^{v=0}_{203,79}} = 1.007 \\ \hline \dfrac{c_{2\ 205,81}}{c_{2\ 203,81}} = 1.005 & \dfrac{g_{205}}{g_{203}} \dfrac{B^{v=0}_{205,81}}{B^{v=0}_{203,81}} = 1.007 \end{cases}$$

As seen by comparing the corresponding ratios in each row, agreement is quite good, which implies that the change in the spin-rotation interaction constants with isotope is understood in terms of the proportionality $c_1 \propto g_i B$.

V.C.3. Vibrational State Dependence of c_1 and c_2

Since c_i is proportional to the rotational constant, B, the change in c_1 and c_2 with vibrational state is expected to be due entirely to the change in B_v with v. This assumption leads to the expression

$$c_i(v) = \frac{c_i(v=0)}{B_o} B_v \ . \qquad V(19)$$

In Figure V(3) we have plotted the calculated values of $c_i(v)$ as a function of v for the molecules $^{205}Tl^{79}Br$ and $^{205}Tl^{81}Br$ as obtained from the J = 2 spectra. The solid lines represent the predicted behavior of $c_i(v)$ on the basis of Eq. V(19). The agreement is seen to be excellent, confirming our expectations.

V.D. Spin-Spin Interactions

The coupling constant for the tensor part of the spin-spin interactions, c_3, is seen to be fairly small and negative in TlBr [Table IV(3)]. c_3 is the sum of two terms: c_3', the direct part of the interaction, and c_3'', the electron-coupled contribution. c_3' is easily calculated from Eq. II(11). For $Tl^{79}Br$ we find that c_3' is about +1.02 kHz. Thus, from the measured value of c_3, c_3'' is found to be negative in all of the thallium-halides and dominates the direct parts to yield negative values of c_3. The scalar part of the spin-spin interaction, c_4, (also an electron-coupled interaction) is seen to be somewhat larger than c_3'' and again negative ($c_4 \cong -6.5$ kHz). Again, this is the case in all of the

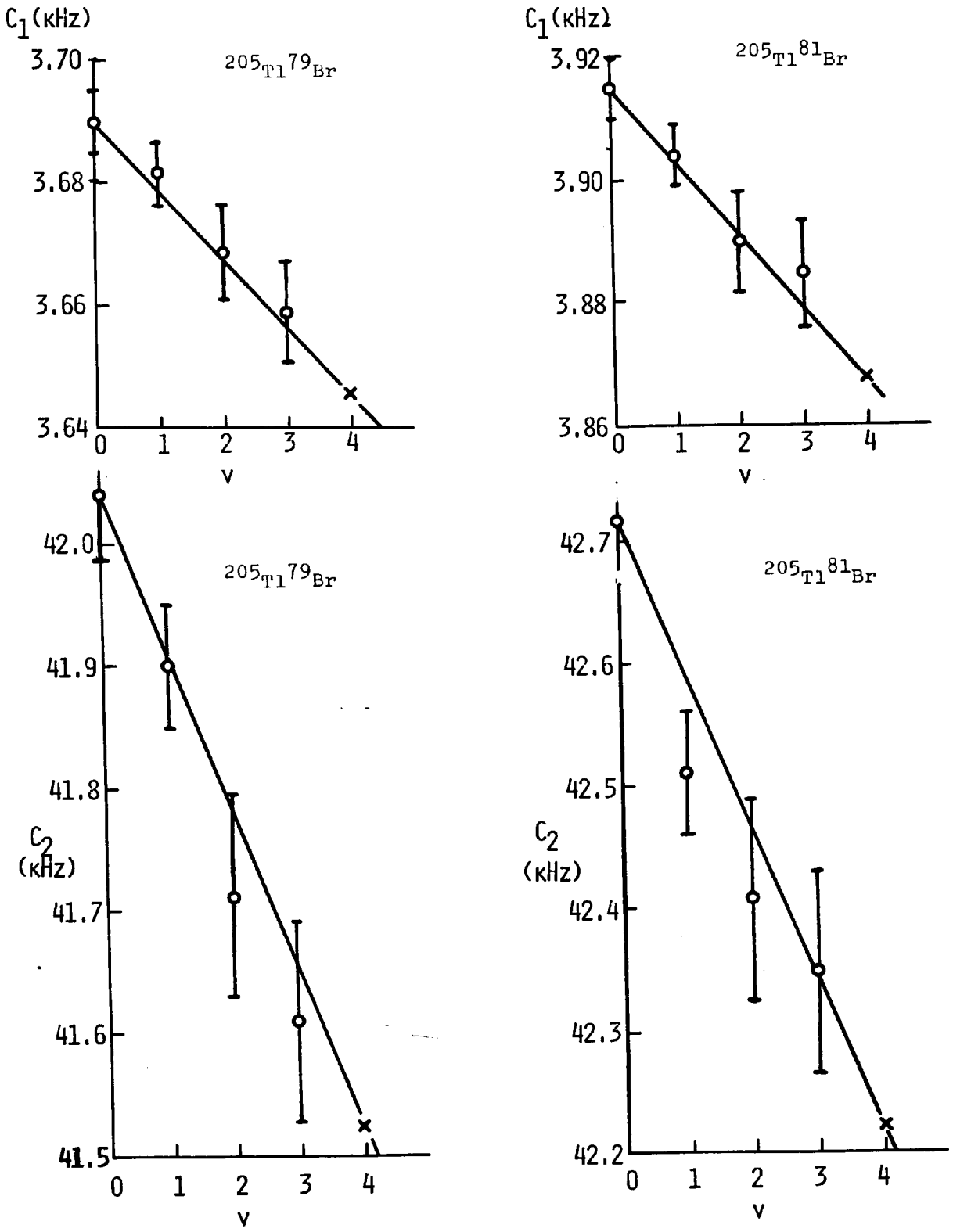


Figure V(3) Dependence of c_1 and c_2 on Vibration State for J = 2, $^{205}Tl^{79}Br$ and $^{205}Tl^{81}Br$.

thallium-halides.

The interpretation of c_3'' and c_4 in terms of the structure of the molecule is quite difficult for molecules such as TlBr. Formal expressions for these quantities are given by Ramsey (1953).

One interesting feature of the three quantities, c_3', c_3'', and c_4, is that they are all proportional to the product of g_{Tl} and g_{Br}. Therefore, by comparing ratios of our measured values of c_3 and c_4 with ratios of the g-factors, we can test for this proportionality. For example, consider the ratios of the J = 2, v = 0 values of c_3 and c_4 for different bromine isotopes (the value of g_{Br} changes by a larger amount than g_{Tl} so that the effect is easier to observe), which are to be compared with g_{79}/g_{81}.

$$c_3 \begin{cases} \dfrac{c_3\ 205,79}{c_3\ 205,81} = 0.929 \\ \dfrac{c_3\ 203,79}{c_3\ 203,81} = 0.930 \end{cases}$$

$$\frac{g_{79}}{g_{81}} = 0.928$$

$$c_4 \begin{cases} \dfrac{c_4\ 205,79}{c_4\ 205,81} = 0.928 \\ \dfrac{c_4\ 203,79}{c_4\ 203,81} = 0.925 \end{cases}$$

The observed agreement of the ratios of the calculated constants with the ratio of g-factors confirms the dependence of c_3 and c_4 on g_{Br}. The dependence of the spin-spin interaction constants on g_{Tl} is also confirmed by our data, although the effect is not as noticeable because of the smaller change in g_{Tl} with Tl isotope.

V.E. Conclusion

Let us summarize what we have accomplished in this investigation. First, we have shown that the hfs of TlBr is well described by the hyperfine Hamiltonian [Eq. II(11)] and the measured interaction constants [Table IV(3)]. This holds true for the spectra of all four isotopic species of TlBr and for the several vibrational and rotational states measured.

Second, from the magnitude of the interaction constants we have obtained such properties of the molecule as the electric field gradient at the bromine nucleus and the magnetic field at both the thallium and bromine nuclei. We have interpreted these quantities in terms of simplified models of the interactions to yield information such as the ionic character of the molecule and the ratio of the electronic orbital angular momenta about the two nuclei. A comparison of some of these properties for all the thallium-halides is given.

Third, we have looked carefully for the existence of false quadrupole effects [Sec.V.A.3.] making use of the full precision of the measured values of eqQ. No substantial

evidence was found for such effects.

Fourth, we have examined the dependence of the quadrupole and spin-rotation interaction constants on vibrational state, and we have been able to interpret these changes in terms of the change of internuclear separation of the molecule with v.

Finally, the measured changes in the magnetic interaction constants with isotopic species have been shown to agree very well with the changes expected from the different nuclear moments and rotational constants.

APPENDIX A

Rectangular Vacuum Chamber

In the design of vacuum enclosures for molecular beam experiments it is quite often desirable to have a long rectangular chamber such that all portions of the inside are easily accessible, and long objects can be placed in and removed from the top without disassembly. The sides of such a chamber may have many penetrations for windows and various feed-throughs with little added cost because of no need of flanged ports. If necessary, small penetrations which could be made with a hand-drill could be added with the chamber situated in its experimental location. Several rectangular boxes have been constructed in our physics department in a way which avoids long welds which have to be vacuum tight. One begins with a flat sheet of 1/2 in. thick brass* which is bent into a U-shaped channel. This is done on a device called a press-brake, using a bending radius of 1-1/2 in. For such bends there is little danger of producing cracks in the brass on the inside or outside of the bend. The Press-Brake available for our work† is

*We have used Muntz metal, which is a brass containing 60% copper and 40% Zinc, simply because it is the most common type available in thick sheets.

†Our bending was done at Fabricating Specialties, 1546 East Nine Mile Road, Hazel Park, Michigan.

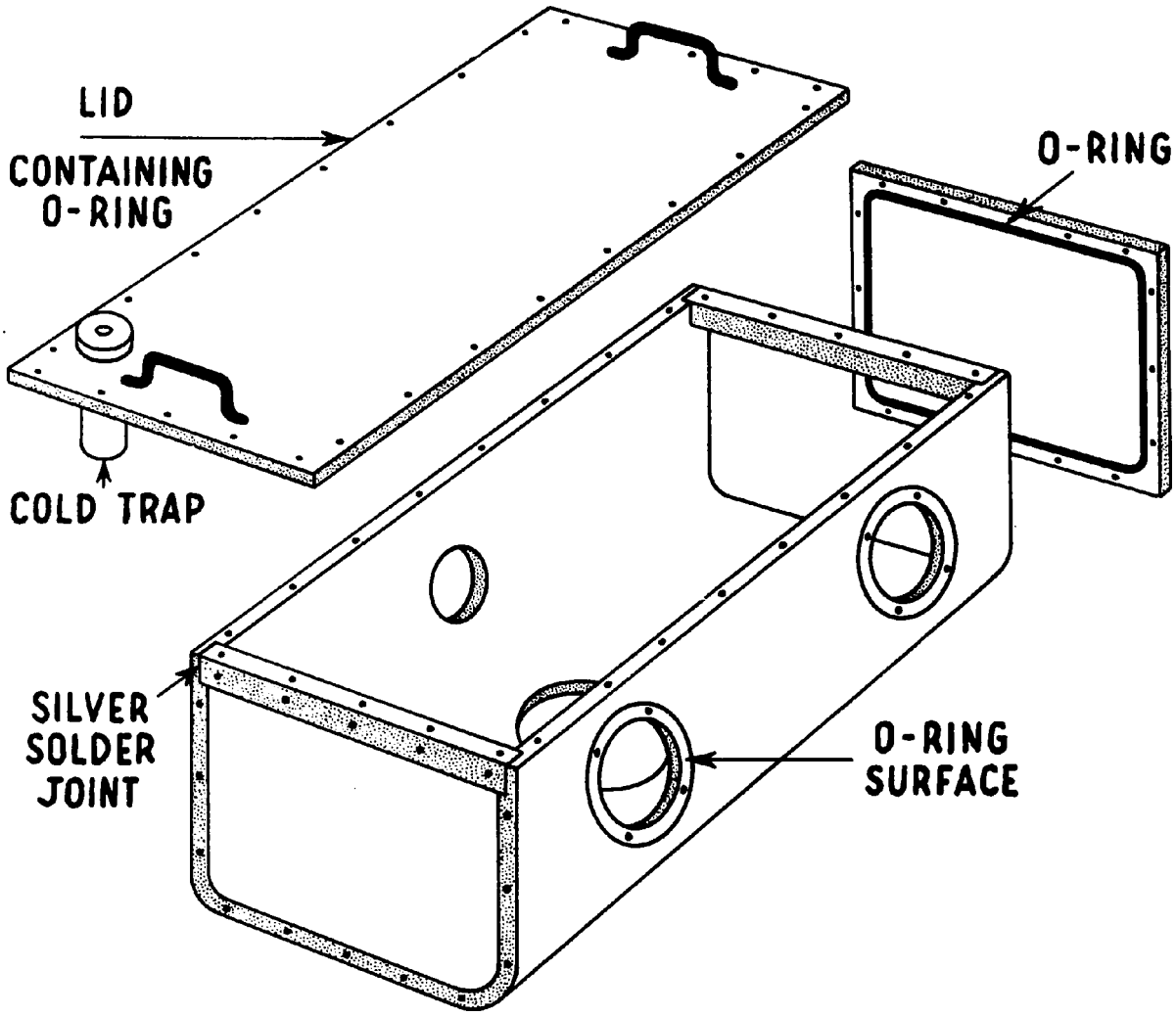


Figure A(1) Rectangular Vacuum Chamber.

capable of bending such channels up to 10 ft. in length. After bending, the channels are annealed at approximately 540° C for two to three hours to partially remove the stresses produced by the bending. During annealing the channel is clamped rigidly to a steel frame to prevent warping.

At each end of the channel, a bar of brass, typically 1 in. square, is silver-soldered into the corners as shown in Figure A(1). Holes are machined in the sides of the channel for access holes, feed-throughs, etc., and in the bottom for diffusion pumps. O-ring surfaces are milled around each hole and polished by hand. Blind bolt holes are drilled and tapped for holding on diffusion pumps and side covers. Retained O-rings* or O-rings contained in the covers are used rather than putting grooves in the chamber. The top and end edges of the chamber are also made into O-ring surfaces, and holes are drilled and tapped for screws along the outside edges. The ends and top of the chamber can be made of any machinable metal, such as aluminum, and also contain the O-rings. It is advisable to make the O-ring grooves the same width as the O-ring so the rings won't fall out of the grooves during assembly. O-rings of abnormal length can be made from stock material which is cut to length and the ends butted together. For neoprene O-rings, Eastman 910 Adhesive† is recommended, and for

---

*For example, Consolidated Vacuum Corporation's "Con-O-Ring".

†A product of Tennessee Eastman Company, Division of Eastman Kodak Company, Kingsport, Tennessee.

Viton one can use Fairprene Cement* Type 5159.

Five such chambers have been constructed and are in use. These range in size from 25 cm x 23 cm x 25 cm to 30 cm x 40 cm x 70 cm and are pumped with 750-2400 liter/sec oil diffusion pumps. With liquid nitrogen cold traps suspended into the chambers from the top, pressures less than 1×10^{-7} torr, as measured with ionization gauges, are obtainable in less than an hour, and ultimate pressures are about 1×10^{-8} torr.

---

*A product of E. I. DuPont De Nemours and Co., Fabrics Division, Fairfield, Connecticut.

APPENDIX B

Focusing Field Equation

The following is a derivation of a useful formula for determining the voltage to apply to a 4-pole electric field to focus a beam of polar molecules. The formula holds for either (1) a source of molecules at a distance L_1 from the entrance to the 4-pole field in which case the molecules leaving the field travel parallel to the symmetry axis of the field, or (2) a beam of molecules traveling parallel to the symmetry axis as they enter the 4-pole field and are focused at a point at a distance L_1 from the exit of the 4-pole field. We will consider the first case. [SeeFigure B(1).]

We make the following assumptions and approximations:

1. The beam consists of molecules moving at the same velocity which we shall assume is:

$$v = 1.33 \sqrt{\frac{2kT}{m}} \qquad B(1)$$

which is the average velocity for molecules of mass m leaving a source at temperature T (°K) through a small hole. k is Boltzmann's constant.

2. The magnitude of the field experienced by the molecules inside the focusing field is

$$|E| = \frac{V}{R_o^2} r \qquad B(2)$$

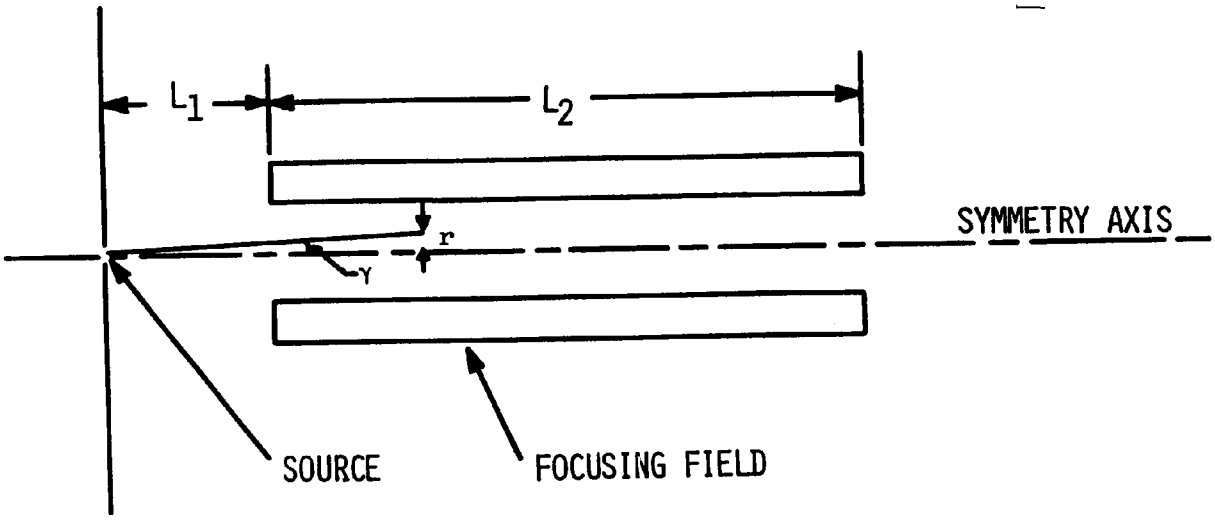


Figure B(1) Schematic Diagram of Beam Source and 4-Pole Focusing Field.

where V is the voltage applied to opposite electrodes, R_o is the distance from the symmetry axis to the inner most edge of the pole pieces, v is the distance of the molecule from the symmetry axis. Equation B(2) holds quite well even for cylindrical electrodes provided $r < 0.8R_o$ and the rod diameter $= (1.15) \cdot (2R_o)$ (Dayton, 1954).

3. The angle γ with which a molecule enters the 4-pole field is assumed small enough to make the approximation $\cos \gamma = 1$.

4. The electric field which the molecule experiences in the focusing field is in the range where its Stark energy does not deviate appreciably from a quadratic dependence on E. This implies that
   a. E is sufficiently large so that the coupling of $\vec{J}$ to $\vec{E}$ is larger than the coupling of $\vec{J}$ to $\vec{I}$, through hyperfine interactions
   b. yet E is not so large that it is necessary to introduce terms of higher order in E, e.g., proportional to E^4, into the Stark energy.

Assumption 4.b. has the effect of limiting the displacement of the molecule from the symmetry axis to such small values of r that assumptions 2 and 3 are automatically satisfied.

$\underline{V_{focus}}$

The force on the molecule in the E field is given by

$$F = - \nabla W_{STARK} \qquad B(3)$$

where in the rigid rotator approximation under assumption 4.b.:

$$W_{STARK} = \frac{\mu^2 E^2}{2B} C \qquad B(4)$$

where

$$C = \frac{J(J+1) - 3M_J^2}{J(J+1)(2J-1)(2J+3)} \qquad B(5)$$

[μ is the permanent electric dipole moment of the molecule, B is the rotational constant, J is the rotational angular momentum quantum number, and M_J is the projection of $\vec{J}$ in the direction of the E field.]

and

$$E^2 = \frac{V^2 r^2}{R_o^4} \qquad B(6)$$

From the above equations, and from the fact that $\ddot{r} = \frac{F}{m}$, we may show that:

$$\ddot{r} = -\sqrt{\frac{a}{m}}\, r \qquad B(7)$$

where

$$a = \frac{\mu^2 V^2}{BR^4} C \qquad B(8)$$

Eq. B(7) has the general solution $r = A \sin\sqrt{\frac{a}{m}}\, t + B \cos\sqrt{\frac{a}{m}}\, t$ B(9)

The boundary conditions are :

a. at $t = 0$ $r + L_1 \tan\gamma$

b. at $t = 0$ $\dot{r} = v \sin\gamma$

The focusing condition is:

c. at $t = \frac{L_2}{v}$, $\dot{r} = 0$.

Conditions a. and b. allow us to evaluate the constants A and B. Substitution of condition c. leads to the expression:

$$\tan \frac{\sqrt{\frac{a}{m}}\, L_2}{v} = \frac{v \cos \gamma}{\frac{a}{m}\, L_1} \qquad B(10)$$

Making the approximation that $\cos \gamma = 1$, and letting

$$y = \frac{\sqrt{\frac{a}{m}}\, L_2}{v} \qquad B(11)$$

yields:

$$\tan y = \frac{L_2}{L_1} \frac{1}{y} \qquad B(12)$$

This transcendental equation may be solved graphically quite simply for a particular $\frac{L_2}{L_1}$. Let y_o be the solution to this equation.

Substituting y_o into the definition of y [Eq. B(11)], writing out a as given by Eq. B(8), and letting $v = 1.33\sqrt{\frac{2kT}{m}}$, we may solve for V, the voltage applied to the 4-pole fields, to obtain:

$$V = \frac{1.33\, y_o\, R^2}{L_2 \mu} \sqrt{\frac{2BkT}{C}} \qquad B(13)$$

Figure B(2) shows the functions $z = \tan y$ and $z = \frac{L_2}{L_1} \frac{1}{y}$ for various values of $\frac{L_2}{L_1}$ near the value 20 (about what this ratio is in our spectrometer) plotted in the region of their intersection. For example, for $\frac{L_2}{L_1} = 20$, we see that $y_o = 1.496$. Equation B(13) is evaluated with this value of y_o, and with $L_2 = 40$ cm, $R = 0.64$ cm, $T = 750\ ^oK$,

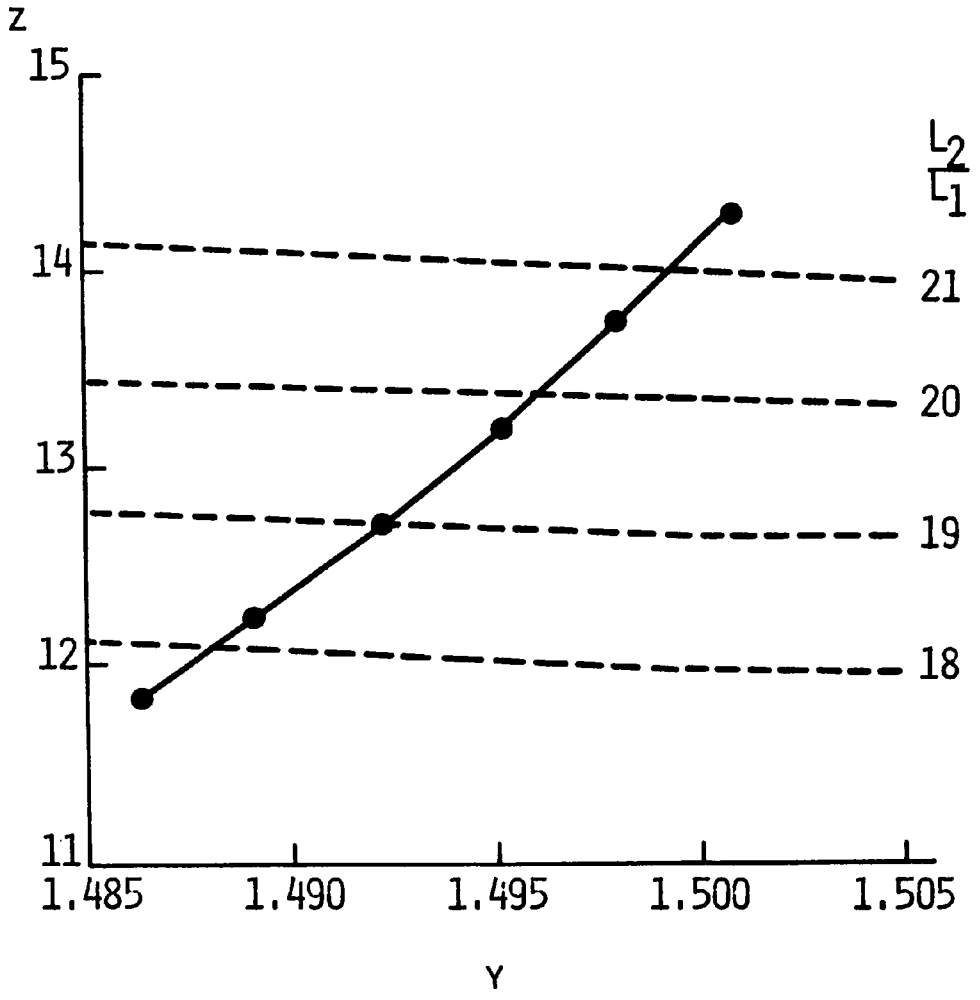


Figure B(2) Graphical Solution to the Transcendental Equation: $\tan y = L_2/L_1 \; 1/y$, for L_2/L_1 in the Neighborhood of 20.

μ = 4.4 Debye, and for the B values of TlCl, TlBr, and TlI, as shown in Table B(1). We use the value of μ which is the measured value of TlCl. The electric dipole moments of TlB and TlI have not been measured, so we make the assumption that they are nearly the same as μ_{TlCl}.

The predicted values of V, shown for various (J, M_J) states that focus, are compared with the voltages, V_{exp}, applied to the focusing fields which yield a maximum in an observed hyperfine transition, the upper hyperfine level of which corresponds to a particular (J, M_J) state. This is expected to be the value of V which deflects the greatest number of molecules in that particular (J, M_J) state onto the detector. (In our spectrometer, the geometry has been chosen so that the A and B-focusing fields require the same voltage, V, to focus the molecules.) In most cases the agreement is quite good. The maxima in the J = 1 signals observed in TlCl and TlI were very broad.

		TlCl		TlBr		TlI	
J	M_J	V (kV)	V_{exp} (kV)	V (kV)	V_{exp} (kV)	V (kV)	V_{exp} (kV)
1	0	6.7	8.0[very broad]	4.4	5[very broad]	3.5	
2	0	12.8	12.5	9.0	9.0	7.2	
3	0	18.9		13.2	13.5	10.5	9.5
4	0	24.7		17.3		13.7	12.5

APPENDIX C

Effective Aperture of Focusing Field

Equation B(13) was derived under the assumption that the Stark energy of the molecule is proportional to the square of the field strength, and higher order terms can be ignored. Bennewitz, Paul, and Schlier (1955) have shown that the effect on molecules experiencing field strengths which are too high (i.e., introducing a substantial E^4 dependence into W_{STARK}) is to focus the molecules with longer focal lengths. If one takes into consideration the finite width of the detector, a criterion for determining the maximum value of E-field that a particular molecule can experience and still hit the detector may be established. The effect of establishing a maximum E is equivalent to restricting the displacement of the molecule from the symmetry axis, since $|E| \sim r$. The restriction of r is in turn equivalent to limiting the aperture at the entrance of the focusing field. Bennewitz, Paul, and Schlier show that the effective aperture, γ^2_{max}, of a 4-pole field is given by:

$$\gamma^2_{max} = \frac{B}{kT} \; -1/2 \; \frac{\mu_{eff}}{\mu} \; (\lambda_{max}) \quad \lambda_{max} \qquad C(1)$$

where B is the rotational constant of the molecule

T is the source temperature in °K

k is Boltzmann's constant

μ_{eff} is the effective dipole moment of the molecule defined by $\mu_{eff} = \frac{-\partial W_{STARK}}{\partial E}$

μ is the permanent dipole moment of the molecule

λ is a dimensionless quantity given by $\lambda = \frac{\mu E}{B}$, so that $\lambda_{max} = \frac{\mu E_{max}}{B}$.

$\frac{\mu_{eff}}{\mu}$ (λ) curves for particular (J,M_J) states are well known (Bennewitz 1955) functions which are properties of rigid, polar rotators independent of diatomic molecule.

Bennewitz, et. al., establish that λ_{max} is to be taken as the value of λ for which the μ_{eff} curve deviates from the tangent to the $\frac{\mu_{eff}}{\mu}$ curve at the origin by 10%

From such a determination of λ_{max} we can use Eq. C(1) to calculate $\frac{kT}{B}\ \gamma^2_{max}$ for the first few focusable (J,M_J) states of TlBr as shown in Table C(1), column 4:

TABLE C(1)

Effective Apertures of Focusing Fields and Observed Intensities

(J,M_J)	λ_{max}	$(-1/2)\frac{\mu_{eff}}{\mu}(\lambda_{max})$	$\frac{kT}{B}\gamma^2_{max}$	$\frac{\gamma^2_{max}(J,M_J)}{\gamma^2_{max}(1,0)}$	$\frac{I(J,M_J)}{I(1,0)}$
(1,0)	.8	0.04	.032	1	1
(2,0)	6.0	0.75	4.5	140	50
(2,1)	2.5	0.025	.06	2	3
(3,0)	10.0	1.8	18	560	30
(3,1)	7.0	0.5	3.5	10	4

In column 5 of Table C(1) we show the effective apertures normalized to the aperture of the J=1, M_J=0 state. Column 6 lists the average intensities of transitions from hyperfine states corresponding to these (J,M_J) states, normalized to J=1, M_J=0.

Comparison of the two columns show moderately good agreement. We have entirely ignored the influence of transition probabilities and alterations of state populations due to diabatic transitions. However, the observations do show the general behavior of the predicted intensities due to the relative aperture, and in particular explain why transitions in the J=1 hfs of TlBr were so difficult to observe.

LIST OF REFERENCES

Barnes, 1954 — R. G. Barnes and W. V. Smith, Phys. Rev. 93, 95 (1954).

Barrett, 1958 — A. H. Barrett and M. Mandel, Phys. Rev. 109, 1572 (1958).

Bennewitz, 1955 — H. G. Bennewitz, W. Paul, and C. Schlier, Z. Physik 141, 6 (1955).

Benz, 1966 — H. P. Benz, A. Bauder, H. Günthard, J. Mol. Spec. 21, 156 (1966).

Bonczyk, 1967 — P. A. Bonczyk and V. W. Hughes, Phys. Rev. 161, 15 (1967).

Brown, 1966 — H. H. Brown and J. G. King, Phys. Rev. 142, 53 (1966).

Carlson, 1952 — R. O. Carlson, C. A. Lee, and B. P. Fabricand, Phys. Rev. 85, 784 (1952).

Dayton, 1954 — I. E. Dayton, F. C. Shoemaker, and R. F. Mozley, Rev. Sci. Instr. 25, 485 (1954).

de Wijn, 1966 — H. W. de Wijn, J. Chem. Phys. 44, 810 (1966).

Edmonds, 1957 — A. R. Edmonds, Angular Momentum in Quantum Mechanics (Princeton University Press, Princeton, 1960), 2nd ed.

English, 1966 — T. C. English, Ph.D. Dissertation, University of Michigan, (University Microfilms, Ann Arbor, Michigan, 1966).

Fitzky, 1958 — H. G. Fitzky, Z. Physik 151, 351 (1958).

Gräff, 1958 — G. Gräff, W. Paul, and C. Schlier, Z. Physik 153, 38 (1958).

Greene, 1961 — E. F. Greene, Rev. Sci. Instr. 32, 860 (1961).

Gunther-Mohr, 1951 — G. R. Gunther-Mohr, S. Geschwind, and C. H. Townes, Phys. Rev. 81, 289L (1951).

Hammerle, 1968 — R. H. Hammerle, J. T. Dickinson, R. G. Van Ausdal, and D. A. Stephenson, Symposium on Molecular Structure and Spectroscopy (Ohio State University, Columbus, Ohio, September, 1968).

Hebert, 1964 — A. J. Hebert, F. W. Breivogel, Jr., and K. Street, Jr., J. Chem. Phys. 41, 2368 (1964). Erratum

H. K. Hughes, 1949 — H. K. Hughes, Phys. Rev. 76, 1675 (1949).

V. W. Hughes, 1950 — V. W. Hughes and L. Grabner, Phys. Rev. 79, 829 (1950).

Kusch, 1959 — P. Kusch and V. W. Hughes, "Atomic and Molecular Beam Spectroscopy," Handbuch der Physik. (Springer-Verlag, Berlin, 1959), Vol. 37/1.

Marple, 1956 — D. T. F. Marple and J. W. Trischka, Phys. Rev. 103, 597 (1956).

Miller, 1966 — C. E. Miller, D. A. Crosby, and J. C. Zorn, Rev. Sci. Instr. 37, 1271, (1966).

Miller, 1967 — C. E. Miller, Ph.D. Dissertation, University of Michigan, (University Microfilms, Ann Arbor, Michigan, 1967).

Moore, 1949 — C. E. Moore, Natl. Bur. Standards (U.S.), Circ. 467 (1949).

Pauling, 1960 — L. Pauling, The Nature of the Chemical Bond (Cornell University Press, Ithaca, 1960), 3rd ed.

Rabi, 1938 — I. I. Rabi, J. R. Zacharias, S. Millman, and R. Kusch, Phys. Rev. 53, 318 (1938).

Ramsey, 1953 — N. F. Ramsey, Phys. Rev. 91, 303 (1953).

Ramsey, 1956 — N. F. Ramsey, Molecular Beams (Oxford University Press, London, 1956).

Schlier, 1957 — C. Schlier, Z. Physik 147, 600 (1957).

Schlier, 1961 — C. Schlier, Fortschr. Physik 9, 455 (1961).

Stephenson, 1968 — D. A. Stephenson, Ph.D. Dissertation, University of Michigan, (University Microfilms, Ann Arbor, Michigan, 1968).

Sternheimer, 1950 — R. Sternheimer, Phys. Rev. 80, 102 (1950).

Svidzinskii, 1964 — K. K. Svidzinskii, Soviet Maser Research (Consultants Bureau, Plenium Press, New York, 1964).

Townes, 1949	C. H. Townes and B. P. Dailey, J. Chem. Phys. 17, 782 (1949).
Townes, 1958	C. H. Townes, "Determination of Nuclear Quadrupole Moments," Handbuch der Physik (Springer-Verlag, Berlin, 1958) Vol. 38/1.
White, 1955	R. L. White, Rev. Mod. Phys. 27, 276 (1955).
Zeiger, 1952	H. J. Zeiger and D. I. Bolef, Phys. Rev. 85, 788 (1952).